PERGAMON

International Journal of Solids and Structures 37 (2000) 2443–2471

INTERNATIONAL JOURNAL OF SOLIDS and STRUCTURES

www.elsevier.com/locate/ijsolstr

Boundary layer realization in thin elastic three-dimensional domains and two-dimensional Hierarchic plate models

M. Dauge[a], Z. Yosibash[b,*]

[a]*Institut Mathématique, UMR 6625 du CNRS, Université de Rennes 1, Campus de Beaulieu, 35042 Rennes, France*
[b]*Pearlstone Center for Aeronautical Engineering Studies, Mechanical Engineering Dept., Ben-Gurion University of the Negev, Beer-Sheva, Israel*

Received 3 September 1998; in revised form 4 December 1998

Abstract

Herein we address the behavior of the linear elastic solution in three-dimensional thin domains, especially near the boundaries, and compare it to the approximated solution obtained by dimension reduced two-dimensional hierarchic plate models. The mathematical analysis is backed-up by numerical simulations using the *p*-version of the finite element method. We identify mathematically, and more importantly, quantify the engineering quantities which are rapidly changing in a boundary layer. We also investigate how well (if at all) the two-dimensional plate-models solutions approximate the three-dimensional solution inside and outside of the boundary layers. © 2000 Elsevier Science Ltd. All rights reserved.

Keywords: Asymptotic analysis; Boundary layers; Thin plates; Hierarchical plate models; *p*-version of the finite element method

1. Introduction

Plates are viewed in structural engineering practice as three-dimensional components with one of their dimensions, usually denoted by 'thickness', much smaller compared to the other two dimensions. Due to the complexity of a three-dimensional elastic analysis, much attention has been given historically to the derivation of 'plate-models', which can be understood as an application of dimensional reduction principles. These plate models are aimed to approximately solve the three-dimensional problem by a two-dimensional formulation, and the most popular models in the engineering practice are the Kirchhoff–Love (K–L) and Reissner–Mindlin (R–M) plate-models. Recently, hierarchic sequence of

* Corresponding author. Tel.: +972-7-647-7103; fax: +972-7-647-2813.
E-mail address: zohary@bgumail.bgu.ac.il (Z. Yosibash)

PII: S0020-7683(99)00004-9

plate-models were proposed so as to make adaptive selection of the model which is best suited for the purpose of a particular quantity of interest.

The quality of the plate-model must be judged on the basis of how well its exact solution approximates the corresponding three-dimensional problem. Especially, of much interest are the boundary layers which may occur in a three-dimensional plate, and their realization (if possible at all) in plate-models. Although several previous works have addressed the existence of boundary layers in plate-models (especially the R–M model), and their treatment by the finite-element method, (Babuška, 1991, 1992a,b; Schwab and Suri, 1996; Arnold and Falk, 1990a, b, 1996) none of the previous publications address in detail the fully three-dimensional solution and its behavior in the boundary layer. Therefore a comparison of the solution in the boundary layer zone between the three-dimensional domain and two-dimensional models is lacking.

Very recent detailed mathematical analysis on the asymptotics in thin three-dimensional elastic plates (Dauge et al., 1997, 1998) makes it possible to identify, and more importantly, quantify the engineering quantities which are rapidly changing in a boundary layer (which is of a magnitude similar to the plate thickness). Furthermore, it is now possible to investigate how well (if at all) the two-dimensional plate-models solutions approximate the three-dimensional solution inside and outside of the boundary layers. To this end, we herein provide explicitly the quantities which exhibit dramatic changes in the boundary layers. We consider the displacements solution in a three-dimensional thin elastic plate of thickness 2ε as an asymptotic inner (in the boundary layer) and outer series of ε. This enables us to investigate and explicitly present which of the engineering quantities are susceptible to radical changes in the boundary layers, and provide visualization of this radical change via numerical experiments as $\varepsilon \longrightarrow 0$.

In Section 2 we provide some notations and preliminaries followed by details on the three-dimensional explicit solution in Section 3. The model problems which are considered for numerical visualization of the mathematical analysis are outlined in Section 4. The mathematical results are demonstrated by numerical experimentation for three-dimensional thin domains in Section 5. We then provide a brief summary on two-dimensional hierarchic plate models in Section 6, followed by various two-dimensional hierarchic plate-model solutions which are compared to the three-dimensional solution and the differences in the behavior especially in boundary layers are emphasized in Section 7. These solutions are obtained using the *p*-version finite element method. We conclude with a summary and conclusions in Section 8.

2. Notations and preliminaries

We denote by $\boldsymbol{u}^{\varepsilon}$ the displacement field in a thin elastic three-dimensional domain Ω^{ε} of thickness 2ε. The domain Ω^{ε} is defined as follows:

$$\Omega^{\varepsilon} = \omega \times (-\varepsilon, +\varepsilon), \quad \text{with } \omega \subset \mathbb{R}^2 \text{ a regular domain.}$$

In general, let $\boldsymbol{u} = (u_1, u_2, u_3)^{\mathrm{T}}$ denote the displacement field, and let $\boldsymbol{e}$ denote the associated linearized strain tensor $e_{ij} = \frac{1}{2}(\partial_i u_j + \partial_j u_i)$, where $\partial_i \equiv \partial/\partial x_i$. The stress tensor $\boldsymbol{\sigma}$ is given by Hooke's law

$$\boldsymbol{\sigma} = [A]\boldsymbol{e},$$

where $[A] = (A_{ijkl})$ is the compliance tensor of an isotropic material expressed in terms of the Lamé constants λ and μ:

$$A_{ijkl} = \lambda\delta_{ij}\delta_{kl} + \mu\left(\delta_{ik}\delta_{jl} + \delta_{il}\delta_{jk}\right).$$

Table 1
The eight possible lateral homogeneous boundary conditions and their engineering notation

ⓘ	Type	Dirichlet	Neumann	$A_{ⓘ}$	$B_{ⓘ}$
①	Hard clamped	$\boldsymbol{u}=0$,		$\{s, n, 3\}$	
②	Soft clamped	$u_n, u_3=0$,	$T_s=0$	$\{n, 3\}$	$\{s\}$
③	Hard simply supported	$u_s, u_3=0$,	$T_n=0$	$\{s, 3\}$	$\{n\}$
④	Soft simply supported	$u_3=0$,	$T_n, T_s=0$	$\{3\}$	$\{s, n\}$
⑤	Frictional I	$u_s, u_n=0$,	$T_3=0$	$\{s, n\}$	$\{3\}$
⑥	Sliding edge	$u_n=0$,	$T_s, T_3=0$	$\{n\}$	$\{s, 3\}$
⑦	Frictional II	$u_s=0$,	T_n, T_3	$\{s\}$	$\{n, 3\}$
⑧	Free		$\boldsymbol{T}=0$		$\{s, n, 3\}$

In the sequel we will use either the Lamé constants or the equivalent engineering material coefficients:

$$\text{Young modulus} \quad E=\frac{\mu(3\lambda+2\mu)}{\lambda+\mu} \text{ and Poisson ratio } \nu=\frac{\lambda}{2(\lambda+\mu)}.$$

The inward traction field on a point of the boundary is $\boldsymbol{T}=(T_1, T_2, T_3)^{\mathrm{T}}$ and defined as $\boldsymbol{\sigma}\cdot\boldsymbol{n}$ where $\boldsymbol{n}$ is the unit interior normal to the boundary.

For simplicity of presentation it is assumed that the boundary conditions on the upper and lower faces of the plate, i.e., $x_3=\pm\varepsilon$, are traction free, and on the lateral faces

$$\partial\Omega_{\mathrm{L}}{}^{\varepsilon}=\partial\omega\times(-\varepsilon,\ +\varepsilon),$$

one of the eight possible combinations of homogeneous boundary conditions denoted by ⓘ where $\mathbf{i}=1,\ldots,8$ are prescribed. The eight different lateral boundary conditions are combinations of three homogeneous displacements or tractions: normal, horizontal tangential and vertical.

To $\boldsymbol{u}$ we associate its horizontal tangential component $u_s:=u_1n_2-u_2n_1$ and its normal component $u_n:=\boldsymbol{u}\cdot\mathbf{n}=u_1n_1+u_2n_2$ on $\partial\Omega_{\mathrm{L}}{}^{\varepsilon}$, the vertical component being u_3 and similar notations apply to $\boldsymbol{T}$. To each boundary condition ⓘ corresponds two complementary sets of indices $A_{ⓘ}$ and $B_{ⓘ}$ where $A_{ⓘ}$ is attached to the Dirichlet conditions of ⓘ, i.e. $u_a=0$ for each index $a\in A_{ⓘ}$. The Neumann conditions are $T_b=0$ for each index $b\in B_{ⓘ}$. Table 1 shows the eight possible lateral boundary conditions.

To each boundary condition ⓘ we associate a space of kinematically admissible displacements:

$$V_{ⓘ}(\Omega^{\varepsilon})=\left\{\boldsymbol{v}\in\left[H^1(\Omega^{\varepsilon})\right]^3;\quad v_a=0 \text{ on } \partial\Omega_{\mathrm{L}}{}^{\varepsilon}\quad\forall a\in A_{ⓘ}\right\}.$$

Then, the weak formulation of the elasticity problem in the three-dimensional domain is stated:

$$\begin{cases}\text{Seek } \boldsymbol{u}^{\varepsilon}\in V_{ⓘ}(\Omega^{\varepsilon}), \quad \text{such that}\\ \displaystyle\int_{\Omega^{\varepsilon}} Ae(\boldsymbol{u}^{\varepsilon}):e(\boldsymbol{v})=\int_{\Omega^{\varepsilon}}\boldsymbol{f}^{\varepsilon}\cdot\boldsymbol{v}, \quad \forall\boldsymbol{v}\in V_{ⓘ}(\Omega^{\varepsilon}),\end{cases} \tag{2.1}$$

where $\boldsymbol{f}^{\varepsilon}$ represents the volume distributed force.

Noting by Greek index α the values in $\{1, 2\}$ corresponding to the in-plane variables, we can state the strong formulation equivalent to (2.1) of the three-dimensional plate problem in Ω^{ε} as

$$(\lambda+\mu)\partial_{\alpha}\,\mathrm{div}\,\boldsymbol{u}^{\varepsilon}+\mu\Delta u_{\alpha}^{\varepsilon}=-f_{\alpha}^{\varepsilon}, \quad \alpha=1,2,$$

$$(\lambda+\mu)\partial_3\,\mathrm{div}\,\boldsymbol{u}^{\varepsilon}+\mu\Delta u_3^{\varepsilon}=-f_3^{\varepsilon}$$

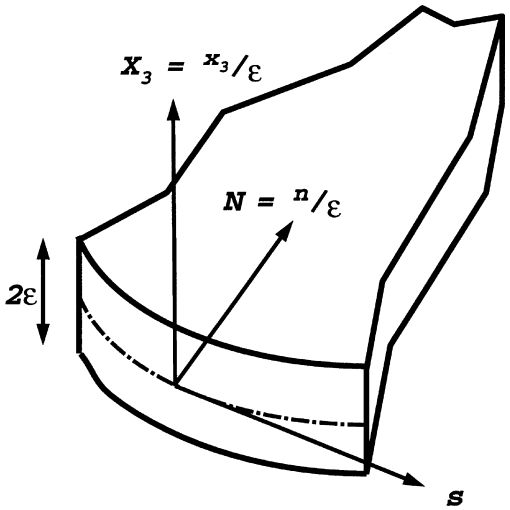

Fig. 1. The coordinate system near plate's lateral boundary.

with traction free boundary conditions on the top and bottom faces of the plate $x_3 = \pm\varepsilon$:

$$2\mu e_{\alpha 3}\boldsymbol{u}^\varepsilon = 0, \quad \alpha = 1,2,$$

$$2\mu\partial_3 u_3^\varepsilon + \lambda \operatorname{div} \boldsymbol{u}^\varepsilon = 0.$$

The boundary conditions on the lateral side $\partial\Omega_L{}^\varepsilon$ are

$$u_a^\varepsilon = 0, \quad \forall a \in A_{\textcircled{i}} \quad \text{and} \quad T_b^\varepsilon = 0, \quad \forall b \in B_{\textcircled{i}}.$$

To examine the behavior of the engineering quantities of interest as $\varepsilon \to 0$, we scale the x_3 coordinate by a factor of $1/\varepsilon$, to obtain a standard domain $\Omega = \omega \times (-1, 1)$. Because we are interested in the lateral boundary layers in the neighborhood of $\partial\omega$, we introduce the new scaled parameter $N = n/\varepsilon$, where n is an axis inward and normal to the boundary, and we also define $X_3 = x_3/\varepsilon$, see Fig. 1. The curvature radius of $\partial\omega$ inside ω at s is denoated by $R = R(s)$, and we recall that $1/R = \kappa$ is the curvature. Notice that for straight boundaries $\kappa = 0$.

Like in Dauge et al. (1997, 1998), we assume that the body forces behave like fixed profiles in the scaled vertical variable X_3 and that they are of order of ε in the vertical direction, namely

$$f_\alpha^\varepsilon(x) = f_\alpha(x_1, x_2, X_3), \quad \alpha = 1, 2, \qquad f_3^\varepsilon(x) = \varepsilon f_3(x_1, x_2, X_3) \tag{2.2}$$

with the data $\boldsymbol{f} = (f_1, f_2, f_3)^{\mathrm{T}}$ regular up to the boundary, i.e. $\boldsymbol{f} \in C^\infty(\bar{\Omega})^3$. These assumptions ensure that the displacements have an asymptotic expansion as $\varepsilon \to 0$ as discussed in the next section, and that this expansion starts 'near' ε^0. Note that, as we are in the framework of linearized elasticity, by superposition we can construct displacement asymptotics for any body forces in the form $\Sigma_k \varepsilon^k \boldsymbol{f}^k(x_1, x_2, X_3)$. Moreover any force which can be expanded as a series $\Sigma_k \varepsilon^k g^k(x_1, x_2, X_3)$ of smooth functions in the unscaled variables (x_1, x_2, X_3), has also the previous form.

The condensed notation $\boldsymbol{u}_*$ is used for $(u_1, u_2)^{\mathrm{T}}$, $\operatorname{div}_* \boldsymbol{u}_*$ denotes $\partial_1 u_1 + \partial_2 u_2$ and Δ_* denotes the horizontal Laplacian $\partial_{11} + \partial_{22}$.

3. Three-dimensional solution

The displacement $\boldsymbol{u}^\varepsilon$ in Ω^ε can be split into a bending part $\boldsymbol{u}^\varepsilon_{\rm b}$ and a membrane (or stretching) part $\boldsymbol{u}^\varepsilon_{\rm m}$, cf Friedrichs and Dressler (1961), according to

$$u^\varepsilon_{{\rm b},\alpha}(x_3) = \tfrac{1}{2}\big(u^\varepsilon_\alpha(x_3) - u^\varepsilon_\alpha(-x_3)\big), \quad \alpha = 1,2, \quad u^\varepsilon_{{\rm b},3}(x_3) = \tfrac{1}{2}\big(u^\varepsilon_3(x_3) + u^\varepsilon_3(-x_3)\big)$$

$$u^\varepsilon_{{\rm m},\alpha}(x_3) = \tfrac{1}{2}\big(u^\varepsilon_\alpha(x_3) + u^\varepsilon_\alpha(-x_3)\big), \quad \alpha = 1,2, \quad u^\varepsilon_{{\rm m},3}(x_3) = \tfrac{1}{2}\big(u^\varepsilon_3(x_3) - u^\varepsilon_3(-x_3)\big)$$

Thus the in-plane components of $\boldsymbol{u}^\varepsilon_{\rm b}$ are odd with respect to x_3 and its vertical component is even, whereas the in-plane components of $\boldsymbol{u}^\varepsilon_{\rm m}$ are even and its vertical component is odd. Of course, $\boldsymbol{u}^\varepsilon_{\rm b}$ is the solution of (2.1) corresponding to the bending part of the body forces $\boldsymbol{f}^\varepsilon_{\rm b}$ and similarly for the membrane.

3.1. Full expansion of displacements

The bending and membrane parts of the displacement $\boldsymbol{u}^\varepsilon$ solution of (2.1) can be expanded in the following way in the sense of asymptotic expansions[1]

$$\boldsymbol{u}^\varepsilon_{\rm b} \simeq \frac{1}{\varepsilon}\boldsymbol{u}^0_{\rm KL,b} + \boldsymbol{u}^1_{\rm KL,b} + \varepsilon\Big(\boldsymbol{u}^2_{\rm KL,b} + \boldsymbol{v}^1_{\rm b} + \boldsymbol{\varphi}^1_{\rm b}\Big) + \cdots + \varepsilon^k\Big(\boldsymbol{u}^{k+1}_{\rm KL,b} + \boldsymbol{v}^k_{\rm b} + \boldsymbol{\varphi}^k_{\rm b}\Big)\cdots \tag{3.1}$$

$$\boldsymbol{u}^\varepsilon_{\rm m} \simeq \boldsymbol{u}^0_{\rm KL,m} + \varepsilon\Big(\boldsymbol{u}^1_{\rm KL,m} + \boldsymbol{v}^1_{\rm m} + \boldsymbol{\varphi}^1_{\rm m}\Big) + \cdots + \varepsilon^k\Big(\boldsymbol{u}^k_{\rm KL,m} + \boldsymbol{v}^k_{\rm m} + \boldsymbol{\varphi}^k_{\rm m}\Big)\cdots \tag{3.2}$$

where

- the $\boldsymbol{u}^k_{\rm KL,b}$ and $\boldsymbol{u}^k_{\rm KL,m}$ are bending and membrane parts of Kirchhoff–Love displacements and are given as:

$$\boldsymbol{u}^k_{\rm KL,b} = \Big(-x_3\partial_1\zeta^k_3,\ -x_3\partial_2\zeta^k_3,\ \zeta^k_3\Big)^{\rm T} \quad \text{and} \quad \boldsymbol{u}^{\rm k}_{\rm KL,m} = \Big(\zeta^k_1,\ \zeta^k_2,\ 0\Big)^{\rm T} \tag{3.3}$$

  where ζ^k_1, ζ^k_2 and ζ^k_3 are functions of the in-plane variables x_* and are denoted by 'generators' because all terms in (3.1)–(3.2) can be generated by ζ^k.

  —The first two terms $\boldsymbol{u}^0_{\rm KL,b}$ and $\boldsymbol{u}^0_{\rm KL,m}$ are the well-known limit Kirchhoff–Love displacement vectors (Ciarlet, 1990).
  —The $\mathcal{O}(1)$ term $\boldsymbol{u}^1_{\rm KL,b}$ manifests the boundary layer profile 'pollution' inside the plate, i.e. away from the boundary.

- The $\boldsymbol{v}^k_{\rm b}$ and $\boldsymbol{v}^k_{\rm m}$ are bending and membrane parts of a displacement $\boldsymbol{v}^k = \boldsymbol{v}^k(x_*, x_3)$ with zero mean value:

$$\forall x_* \in \bar{\omega}\,, \int_{-1}^{+1} \boldsymbol{v}^k(x_*, X_3)\,{\rm d}X_3 = 0$$

  It is important to notice that $\boldsymbol{v}^k$ does not depend on ε;

[1] This means that the difference between the solution of (2.1) and the truncated series of (3.1)–(3.2) at the order k is estimated by $c_k\varepsilon^{k+1}$, cf more precisely (Dauge et al., 1997, 1998).

- the $\boldsymbol{\varphi}^k_{\mathrm{b}}$ and $\boldsymbol{\varphi}^k_{\mathrm{m}}$ are bending and membrane parts of a bounded boundary layer profile $\boldsymbol{\varphi}^k = \boldsymbol{\varphi}^k(s, N, X_3)$ exponentially decreasing as $N \to \infty$.

We give more information about these different terms.

3.1.1. The Kirchhoff–Love displacements

$\boldsymbol{u}^k_{\mathrm{KL,m}}$ and $\boldsymbol{u}^k_{\mathrm{KL,b}}$ are determined by three functions defined on ω: $(\zeta^k_1, \zeta^k_2)^{\mathrm{T}} = \boldsymbol{\zeta}^k_*$ and ζ^k_3, respectively. The in-plane displacement $\boldsymbol{\zeta}^k_*$ is the solution of the 'membrane equation':

$$\mu[\Delta_*]\boldsymbol{\zeta}^k_* + (\tilde{\lambda} + \mu)\nabla_* \mathrm{div}_* \boldsymbol{\zeta}^k_* = \boldsymbol{R}^k_{\mathrm{m}}, \tag{3.4}$$

whereas ζ^k_3 solves the 'bending equation':

$$(\tilde{\lambda} + 2\mu)\Delta^2_* \zeta^k_3 = R^k_{\mathrm{b}}, \tag{3.5}$$

with $\tilde{\lambda} = 2\lambda\mu(\lambda + 2\mu)^{-1}$ and $[\Delta_*]$ the vectorial horizontal Laplacian. The right hand side of (3.4) for $\boldsymbol{\zeta}^0_*$ is given by:

$$\boldsymbol{R}^0_{\mathrm{m}}(\boldsymbol{x}_*) = -\frac{1}{2}\int_{-1}^{+1} \boldsymbol{f}_*(x_*, X_3)\, \mathrm{d}X_3$$

and the right hand side of (3.5), for ζ^0_3 is:

$$R^0_{\mathrm{b}}(\boldsymbol{x}_*) = \frac{3}{2}\left[\int_{-1}^{+1} f_3\, \mathrm{d}X_3 + \mathrm{div}_*\left(\int_{-1}^{+1} X_3 \boldsymbol{f}_*\, \mathrm{d}X_3\right)\right]$$

and for $\boldsymbol{\zeta}^k$, $k = 1, 2, \ldots$ the right hand sides are provided in Table 6 in Dauge et al. (1997) Part I or in Table 5 Dauge et al. (1997) Part II.

The type of boundary conditions on $\partial\omega$ for the generators are provided in Tables 2 and 3 in Dauge et al. (1997), and we only remark on several interesting properties:

—For the four cases ①, ②, ③, and ④, (unlike the other four cases) the boundary conditions for the partial differential equations involving $\boldsymbol{\zeta}^0$ are all 0.
—The boundary conditions for $\boldsymbol{\zeta}^1$ are special traces of $\boldsymbol{\zeta}^0$ according to Table 3 in Dauge et al. (1997). It is important to note that the boundary conditions consist of traces associated with the boundary layer profiles, hence, the boundary layers influence $\boldsymbol{\zeta}^1$ through these boundary conditions.
—For the four cases ⑤, ⑥, ⑦, and ⑧, $\zeta^1_1 = \zeta^1_2 = 0$.

3.1.2. The first displacements $\boldsymbol{v}^1$

The displacement vectors $\boldsymbol{v}^1_{\mathrm{b}}$ and $\boldsymbol{v}^1_{\mathrm{m}}$ are also completely determined by $\boldsymbol{\zeta}^0$, and their expressions are given by:

$$\boldsymbol{v}^1_{\mathrm{b}}(\boldsymbol{x}_*, X_3) = \frac{\nu}{6(1-\nu)}\left(0, 0, (3X_3^2 - 1)\Delta_* \zeta^0_3\right)^{\mathrm{T}}, \tag{3.6}$$

$$\boldsymbol{v}^1_{\mathrm{m}}(\boldsymbol{x}_*, X_3) = \frac{\nu}{6(1-\nu)}\left(0, 0, -6X_3\, \mathrm{div}_* \boldsymbol{\zeta}^0_*\right)^{\mathrm{T}}. \tag{3.7}$$

3.1.3. The boundary layer first profiles for cases ①, ②, ③, and ④

$\boldsymbol{\varphi}^1_{\mathrm{b}}$ can be described as a sum of two terms in tensor product form in the variables s and (N, X_3):

$$\boldsymbol{\varphi}^1_{\mathrm{b}} = a(s)\boldsymbol{\varphi}^{1a}_{\mathrm{b}}(N, X_3) + b(s)\boldsymbol{\varphi}^{1b}_{\mathrm{b}}(N, X_3), \tag{3.8}$$

whereas $\boldsymbol{\varphi}^1_{\mathrm{m}}$ has an expression in tensor product form

$$\boldsymbol{\varphi}^1_{\mathrm{m}} = c(s)\boldsymbol{\varphi}^{1c}_{\mathrm{m}}(N, X_3) \tag{3.9}$$

Here $\boldsymbol{\varphi}^{1a}_{\mathrm{b}}$, $\boldsymbol{\varphi}^{1b}_{\mathrm{b}}$ and $\boldsymbol{\varphi}^{1c}_{\mathrm{m}}$ are typical profiles whose components in the horizontal tangent, normal and vertical directions have special behaviors with respect to X_3:

$$\boldsymbol{\varphi}^{1a}_{\mathrm{b}} = (0, \text{odd}, \text{even})^{\mathrm{T}}$$

$$\boldsymbol{\varphi}^{1b}_{\mathrm{b}} = (\text{odd}, 0, 0)^{\mathrm{T}}$$

$$\boldsymbol{\varphi}^{1c}_{\mathrm{m}} = (0, \text{even}, \text{odd})^{\mathrm{T}}$$

The functions a, b, c are given as traces of $\boldsymbol{\zeta}^0$ along the boundary $\partial\omega$ according to the Table 2a.

Note the presence of κ in front of the traces for the hard simple support case; the existence of boundary layer terms is linked to non zero curvature.

3.1.4. The boundary layer first profile for cases ⑤, ⑥, ⑦, and ⑧

In contrast to the previous four 'clamped' lateral boundary conditions, the normal and transverse components of $\boldsymbol{\varphi}^1$ are zero, i.e. $\varphi^1_N = \varphi^1_3 = 0$, and the only nonzero component is $\varphi^1_{\mathrm{b},s}$. Moreover, $\boldsymbol{\varphi}^1_{\mathrm{m}} = 0$. $\boldsymbol{\varphi}^1_{\mathrm{b}}$ is still given by (3.8), with $a(s) = 0$ and $b(s)$ is given according to Table 2b.

3.1.5. The relation between curvature and boundary layer first profiles

There are boundary conditions for which boundary layers do not develop in case the boundary is straight. These are ③ and ⑥. Boundary layers always develop for curved boundaries. A summary of the cases at which boundary layers do appear are given in Table 3. The letters s, N, X_3 denote if boundary layers are in the horizontal tangential, normal or vertical component of the displacement fields.

Table 2a
Values of $a(s)$, $b(s)$ and $c(s)$ for ①–④ BCs

Case	$a(s)$	$b(s)$	$c(s)$
① and ②	$\Delta_* \zeta^0_3$	0	$\mathrm{div}_* \boldsymbol{\zeta}^0_*$
③	$\kappa \partial_n \zeta^0_3$	0	$\kappa \zeta^0_n$
④	$\kappa \partial_n \zeta^0_3$	$\partial_s(\partial_n \zeta^0_3)$	$\mathrm{div}_* \boldsymbol{\zeta}^0_*$

Table 2b
Value of $b(s)$ for ⑤–⑧ BCs

Case	$b(s)$
⑤	$\partial_s \zeta^0_3$
⑥	$\kappa \partial_s \zeta^0_3$
⑦	$\partial_s \zeta^0_3$
⑥	$(\partial_n + \kappa)\partial_s \zeta^0_3$

Table 3
Existence of boundary layers for the eight possible lateral homogeneous boundary conditions

ⓘ	Type	Straight boundary	Curved boundary
①	Hard clamped	N, X_3	N, X_3
②	Soft clamped	N, X_3	N, X_3
③	Hard simply supported	—	N, X_3
④	Soft simply supported	s, N, X_3	s, N, X_3
⑤	Frictional I	s	s
⑥	Sliding edge	—	s
⑦	Frictional II	s	s
⑧	Free	s	s

3.2. First terms of displacements

To realize the specific quantities which play a significant role in each of the various zones in the thin plate we present herein the first terms in the expansion (3.1)–(3.2), up to $\mathcal{O}(\varepsilon^2)$. Throughout the plate $x_3/\varepsilon \equiv X_3$, see Fig. 1.

To visualize which of the values approach zero as $\varepsilon \to 0$, we express these in terms of the $\mathcal{O}(1)$ variables s, N, X_3 used in the boundary layer and x_1, x_2, X_3 used elsewhere. With this in mind, (3.1)–(3.2) take the form:

$$\boldsymbol{u}^{\varepsilon}_{\mathrm{b}} = \begin{bmatrix} -X_3\partial_1\zeta^0_3 & -\varepsilon X_3\partial_1\zeta^1_3 & +0 & +0 \\ -X_3\partial_2\zeta^0_3 & -\varepsilon X_3\partial_2\zeta^1_3 & +0 & +0 \\ \dfrac{1}{\varepsilon}\zeta^0_3 & +\zeta^1_3 & +\varepsilon\zeta^2_3 & \varepsilon v^1_{\mathrm{b},3} \end{bmatrix} + \varepsilon\boldsymbol{\varphi}^1_{\mathrm{b}} + \mathcal{O}(\varepsilon^2) \tag{3.10}$$

$$\boldsymbol{u}^{\varepsilon}_{\mathrm{m}} = \begin{pmatrix} \zeta^0_1 & +\varepsilon\zeta^1_1 & +0 \\ \zeta^0_2 & +\varepsilon\zeta^1_2 & +0 \\ 0 & +0 & +\varepsilon v^1_{\mathrm{m},3} \end{pmatrix} + \varepsilon\boldsymbol{\varphi}^1_{\mathrm{m}} + \mathcal{O}(\varepsilon^2) \tag{3.11}$$

where the symbol $\mathcal{O}(\varepsilon^2)$ means that the remainder is uniformly bounded by $c\varepsilon^2$ and $\boldsymbol{\varphi}^1$ is determined according to the eight canonical cases in (3.8)–(3.9).

Examining (3.10)–(3.11) it may be noticed that the displacement field is dominated by the Kirchhoff–Love components, and especially the vertical bending component of $\boldsymbol{u}^0_{\mathrm{KL,b}}$ is much larger than any other displacement component (this is commonly known). However, in order to visualize the boundary layer effects in the bending displacement field, we filter out constants in X_3 by the introduction of the quantities, defined in the neighborhood of ω's boundary:

$$J_i[\boldsymbol{u}](s, N) = \frac{1}{\varepsilon}\int_{-\varepsilon}^{\varepsilon} \frac{u_3(s, N, X_3)}{\varepsilon} P_i\left(\frac{x_3}{\varepsilon}\right) \mathrm{d}x_3$$

$$= \frac{1}{\varepsilon}\int_{-1}^{+1} u_3\,(s, N, X_3) P_i(X_3)\,\mathrm{d}X_3, \quad i = 2, 4, 6 \tag{3.12}$$

where $P_i(t)$ is the Legendre polynomial of order i. Because ζ_3^0, ζ_3^1 and ζ_3^2 are constants in respect to x_3, then they are orthogonal to P_i ($i \neq 0$). Computing $J_i[\boldsymbol{u}](s, N)$ at a given point s of the boundary along the inward normal $0 \leqslant n/2\varepsilon \leqslant 1$ emphasizes the boundary layers in the displacements fields. Since $v_{\mathrm{b},3}^1$ has a term which depends on X_3^2, see (3.6), then we expect that $J_2[\boldsymbol{u}](s, N)$ will vary in the boundary layer zone due to the effect of the boundary layer profile, but will become constant outside of the boundary layer. This will be demonstrated numerically in Section 5.

3.3. First terms of strains

A more pronounced influence of the boundary layers shows up when examining the strain components. We herein denote the bending and membrane strain vectors associated with $\boldsymbol{u}_{\mathrm{b}}$ and $\boldsymbol{u}_{\mathrm{m}}$, respectively, by

$$\boldsymbol{e}_{\mathrm{b}} = (e_{\mathrm{b},11}\ e_{\mathrm{b},22}\ e_{\mathrm{b},33}\ e_{\mathrm{b},23}\ e_{\mathrm{b},13}\ e_{\mathrm{b},12}\ )^{\mathrm{T}} \quad \text{and} \quad \boldsymbol{e}_{\mathrm{m}} = (e_{\mathrm{m},11}\ e_{\mathrm{m},22}\ e_{\mathrm{m},33}\ e_{\mathrm{m},23}\ e_{\mathrm{m},13}\ e_{\mathrm{m},12})^{\mathrm{T}}.$$

We investigate the strain asymptotics successively outside and inside the boundary layer zone.

3.3.1. Outside the boundary layer zone

In a region of the form $\omega_0 \times (-\varepsilon, \varepsilon)$ where $\bar{\omega}_0 \subset \omega$, the effect of the boundary layer terms is not visible since the $\boldsymbol{\varphi}^k$ are exponentially decreasing. Then the asymptotics of $\boldsymbol{e}_{\mathrm{b}}$ and $\boldsymbol{e}_{\mathrm{m}}$ contains only the terms coming from $\boldsymbol{u}_{\mathrm{KL,b}}^k$, $\boldsymbol{v}_{\mathrm{b}}^k$ and $\boldsymbol{u}_{\mathrm{KL,m}}^k$, $\boldsymbol{v}_{\mathrm{m}}^k$ respectively, namely

$$\begin{bmatrix} e_{\mathrm{b},11} \\ e_{\mathrm{b},22} \\ e_{\mathrm{b},33} \\ e_{\mathrm{b},23} \\ e_{\mathrm{b},13} \\ e_{\mathrm{b},12} \end{bmatrix} = \begin{bmatrix} -X_3\,\partial_{11}\zeta_3^0 & -\varepsilon X_3\,\partial_{11}\zeta_3^1 & +0 \\ -X_3\,\partial_{22}\zeta_3^0 & -\varepsilon X_3\,\partial_{22}\zeta_3^1 & +0 \\ 0 & +0 & +\dfrac{\upsilon}{1-\upsilon}X_3\Delta_*\zeta_3^0 \\ 0 & +0 & +\varepsilon\dfrac{\upsilon}{6(1-\upsilon)}\big(3X_3^2-1\big)\partial_2\Delta_*\zeta_3^0 \\ 0 & +0 & +\varepsilon\dfrac{\upsilon}{6(1-\upsilon)}\big(3X_3^2-1\big)\partial_1\Delta_*\zeta_3^0 \\ -X_3\partial_{12}\zeta_3^0 & -\varepsilon X_3\partial_{12}\zeta_3^1 & +0 \end{bmatrix} + \cdots$$

$$= \begin{bmatrix} -X_3\partial_{11}\zeta_3^0 \\ -X_3\partial_{22}\zeta_3^0 \\ \dfrac{\upsilon}{1-\upsilon}X_3\Delta_*\zeta_3^0 \\ 0 \\ 0 \\ -X_3\partial_{12}\zeta_3^0 \end{bmatrix} + \mathcal{O}(\varepsilon) \tag{3.13}$$

and

$$\begin{bmatrix} e_{\mathrm{m},11} \\ e_{\mathrm{m},22} \\ e_{\mathrm{m},33} \\ e_{\mathrm{m},23} \\ e_{\mathrm{m},13} \\ e_{\mathrm{m},12} \end{bmatrix} = \begin{bmatrix} \partial_1\zeta_1^0 & +\varepsilon\partial_1\zeta_1^1 & +0 \\ \partial_2\zeta_2^0 & +\varepsilon\partial_2\zeta_2^1 & +0 \\ 0 & +0 & -\dfrac{\upsilon}{1-\upsilon}\,\mathrm{div}_*\boldsymbol{\zeta}_*^0 \\ 0 & +0 & -\varepsilon\dfrac{\upsilon}{2(1-\upsilon)}X_3\partial_2\,\mathrm{div}_*\boldsymbol{\zeta}_*^0 \\ 0 & +0 & -\varepsilon\dfrac{\upsilon}{2(1-\upsilon)}X_3\partial_1\,\mathrm{div}_*\boldsymbol{\zeta}_*^0 \\ \dfrac{1}{2}\Big(\partial_2\zeta_1^0+\partial_1\zeta_2^0\Big) & +\varepsilon\dfrac{1}{2}\Big(\partial_2\zeta_1^1+\partial_1\zeta_2^1\Big) & +0 \end{bmatrix} + \cdots$$

$$= \begin{bmatrix} \partial_1\zeta_1^0 \\ \partial_2\zeta_2^0 \\ -\dfrac{\upsilon}{1-\upsilon}\,\mathrm{div}_*\boldsymbol{\zeta}_*^0 \\ 0 \\ 0 \\ \dfrac{1}{2}\Big(\partial_2\zeta_1^0+\partial_1\zeta_2^0\Big) \end{bmatrix} = \mathcal{O}(\varepsilon). \tag{3.14}$$

Thus we can see that, outside the boundary layer zone, the components e_{23} and e_{13} are of order ε, unlike the four other ones in general.

3.3.2. Inside the boundary layer zone

For this reason we investigate more specially the two components e_{23} and e_{13} inside the boundary layer zone in order to make the boundary layer visible. Now, instead of the Cartesian in-plane components, it is more natural to consider the tangential and normal components, namely for the strains

$$e_{s3} = \frac{1}{2}(\partial_s u_3 + \partial_3 u_s) \quad \text{and} \quad e_{n3} = \frac{1}{2}(\partial_n u_3 + \partial_3 u_n).$$

For ①, ② and ③:

$$\begin{pmatrix} e_{\mathrm{b},s3} \\ e_{\mathrm{b},n3} \end{pmatrix} = \begin{pmatrix} 0 \\ \dfrac{1}{2}\Big(\partial_{X_3}\varphi_{\mathrm{b},N}^1 + \partial_N\varphi_{\mathrm{b},3}^1\Big) \end{pmatrix} + \frac{\varepsilon}{2}\begin{pmatrix} \partial_s v_{\mathrm{b},3}^1 \\ \partial_n v_{\mathrm{b},3}^1 \end{pmatrix} + \mathcal{O}(\varepsilon^2) \tag{3.15}$$

and

$$\begin{pmatrix} e_{\mathrm{m},s3} \\ e_{\mathrm{m},n3} \end{pmatrix} = \begin{pmatrix} 0 \\ \dfrac{1}{2}\Big(\partial_{X_3}\varphi_{\mathrm{m},N}^1 + \partial_N\varphi_{\mathrm{m},3}^1\Big) \end{pmatrix} + \frac{\varepsilon}{2}\begin{pmatrix} \partial_s v_{\mathrm{m},3}^1 \\ \partial_n v_{\mathrm{m},3}^1 \end{pmatrix} + \mathcal{O}(\varepsilon^2). \tag{3.16}$$

Thus the strain component e_{n3} is influenced mainly by the boundary layer term which is of order 1, and influenced at the order ε by the $\boldsymbol{v}^1$ term.

For condition ④, we still have (3.16), but instead of (3.15), due to the presence of the new bending tangential component $\varphi_{\mathrm{b},s}^{1b}$ in the boundary layer terms, we have now:

$$\begin{pmatrix} e_{\mathrm{b},s3} \\ e_{\mathrm{b},n3} \end{pmatrix} = \begin{pmatrix} \frac{1}{2}\partial_s \partial_n \zeta_3^0(s) \partial_{X_3} \varphi_{\mathrm{b},s}^{1b} \\ \frac{1}{2}\kappa \partial_n \zeta_3^0(s) \left(\partial_{X_3} \varphi_{\mathrm{b},N}^{1a} + \partial_N \varphi_{\mathrm{b},3}^{1a} \right) \end{pmatrix} + \frac{\varepsilon}{2} \begin{pmatrix} \partial_s \upsilon_{\mathrm{b},3}^1 \\ \partial_n \upsilon_{\mathrm{b},3}^1 \end{pmatrix} + \mathcal{O}(\varepsilon^2). \tag{3.17}$$

Thus $e_{n,3}$ in the boundary layer zone is of order ε for straight boundaries but of order 1 for curved boundaries.

For boundary conditions ⑤–⑧, since $\boldsymbol{\varphi}_{\mathrm{m}}^1 \equiv 0$, only the bending part is of interest:

$$\begin{pmatrix} e_{\mathrm{b},s3} \\ e_{\mathrm{b},n3} \end{pmatrix} = \begin{pmatrix} \frac{1}{2}\partial_{X_3} \varphi_{\mathrm{b},s}^1 \\ 0 \end{pmatrix} + \frac{\varepsilon}{2} \begin{pmatrix} \partial_s \upsilon_{\mathrm{b},3}^1 \\ \partial_n \upsilon_{\mathrm{b},3}^1 \end{pmatrix} + \mathcal{O}(\varepsilon^2) \tag{3.18}$$

Here, the strain component e_{s3} is influenced by the boundary layer term at the order 1, and influenced at the order ε by the $\boldsymbol{\upsilon}^1$ term.

4. Model problems used for demonstration purposes

The theoretical results are visualized by computing functionals associated with the boundary layer terms for the different boundary conditions. We consider two configurations: the first one is a rectangular plate, thus with straight edges; whereas the second one is a circular plate, thus the boundary has a non-zero curvature.

4.1. Rectangular plate

Its dimensions are $4 \times 1 \times 2\varepsilon$ and it is subjected to a *bending* volume force $\boldsymbol{f}^\varepsilon = (0, 0, 2\varepsilon)^{\mathrm{T}}$, see Fig. 2 The material properties are: Poisson ratio $\nu = 1/8$ and Young modulus $E = 27/4$. Being interested in the boundary layers along edge FB of the plate, we keep the other boundaries EF and DB hard clamped, while on the boundaries FB and ED we apply the various eight homogeneous boundary conditions. These boundary conditions give rise to two axes of symmetry, so that only a quarter of the plate may be analyzed, namely plate $ABCG$, with symmetry boundary conditions ⑥ on AG and GC.

We consider a part of this plate which has one of its boundaries along the x_1 axis, so that in the boundary layer zone $x_1 \equiv s$, and $x_2 \equiv N$. Thus, in the neighborhood of the point A, $\partial_1 \equiv \partial/\partial_s$, $\partial_2 \equiv (1/\varepsilon)\partial/\partial N$, and overall the domain $\partial_3 \equiv (1/\varepsilon)\,\partial/\partial X_3$.

To visualize the boundary layer influence we compute the normalized root mean square (N-RMS) norm I_{13}^{bl} of $e_{13} = e_{s3}$ and I_{23}^{bl} of $e_{23} = e_{n3}$ inside the boundary layer zone according to the formula

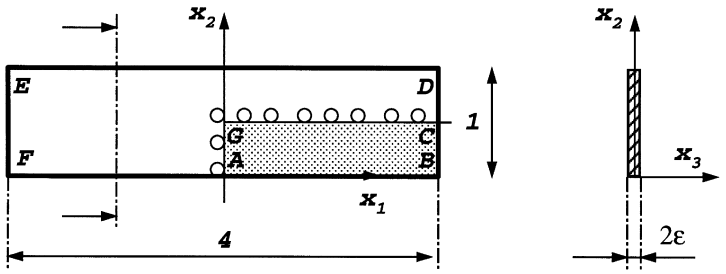

Fig. 2. Rectangular plate under consideration.

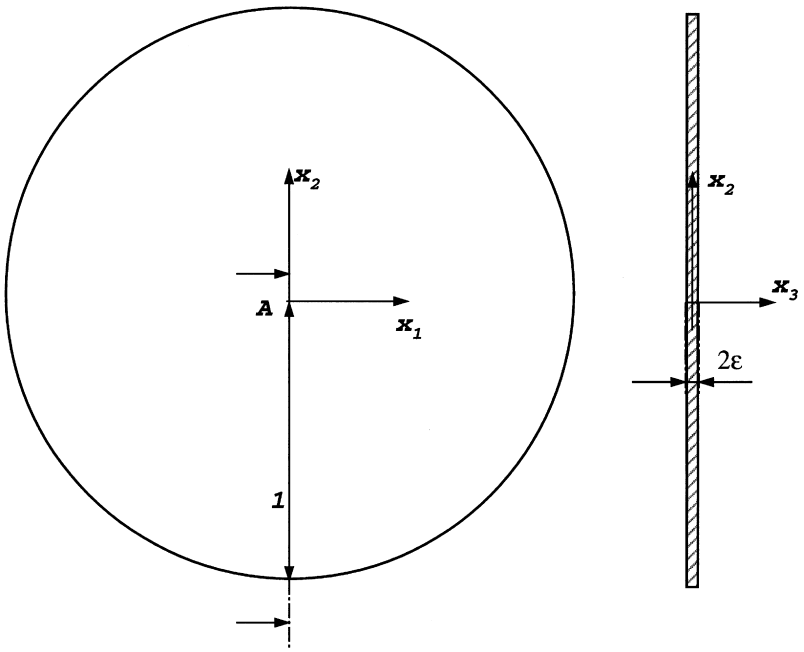

Fig. 3. Circular plate under conideration.

$$I_{\alpha 3}^{\mathrm{bl}} = \sqrt{\frac{1}{V}\int_{x_1=0}^{1}\int_{x_2=0}^{2\varepsilon}\int_{x_3=-\varepsilon}^{\varepsilon} |e_{\alpha 3}|^2 \,\mathrm{d}V}, \quad \alpha = 1, 2, \tag{4.1}$$

and the N-RMS norm of I_{13}^{out} of e_{13} and I_{23}^{out} of e_{23} away from the boundary layer:

$$I_{\alpha 3}^{\mathrm{out}} = \sqrt{\frac{1}{V}\int_{x_1=0}^{1}\int_{x_2=0.25}^{0.5}\int_{x_3=-\varepsilon}^{\varepsilon} |e_{\alpha 3}|^2 \,\mathrm{d}V}, \quad \alpha = 1, 2, \tag{4.2}$$

where V denotes the volume of the 'box' in which the strain components are sought. *The main interest of this N-RMS norm is that it has the same behavior in* ε *as the corresponding strain component*.

4.2. Circular plate

The second configuration under investigation is a circular plate of radius 1 and thickness 2ε as shown in Fig. 3. Material properties and volume force remain unchanged. For this case (of a circular boundary) we define

$$I_{n3}^{\mathrm{bl}} = \sqrt{\frac{1}{V}\int_{r=1-2\varepsilon}^{1}\int_{\theta=0}^{2\pi}\int_{x_3=-\varepsilon}^{\varepsilon} |e_{n3}|^2 r \,\mathrm{d}r \,\mathrm{d}\theta \,\mathrm{d}x_3} \tag{4.3}$$

where V is the volume of the annulus zone $r \in (1 - 2\varepsilon, 1)$ under consideration.

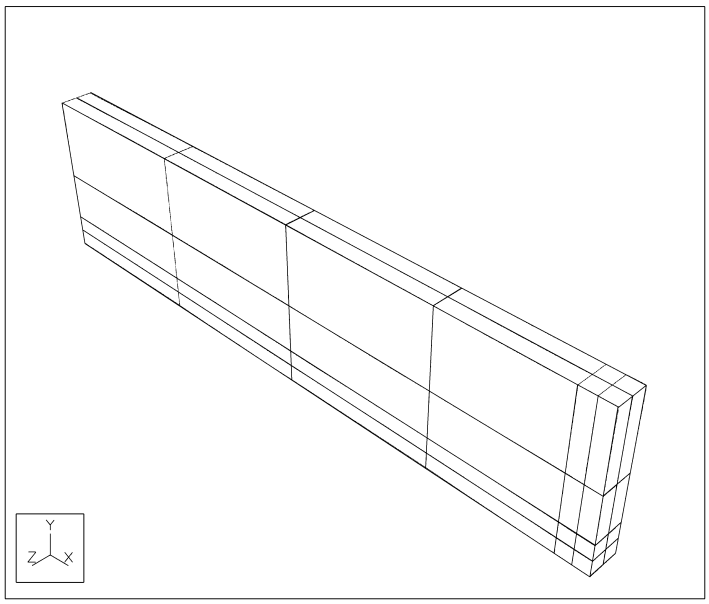

Fig. 4. Finite element mesh for the plate with $2\varepsilon = 0.1$.

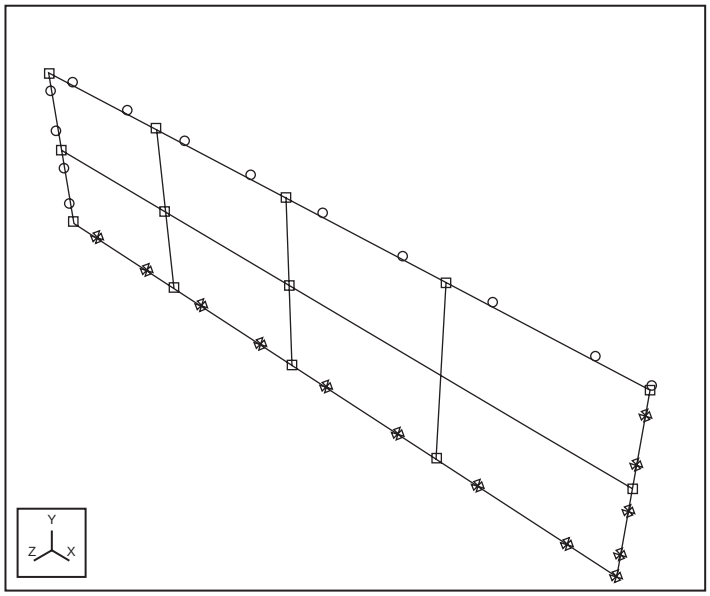

Fig. 5. Finite element mesh and boundary conditions for the plate with $2\varepsilon = 0.001$.

5. Numerical tests for three-dimensional problems

In this section numerical results are provided which demonstrate the solution characteristics inside and outside of the boundary layers in three-dimensional domains.

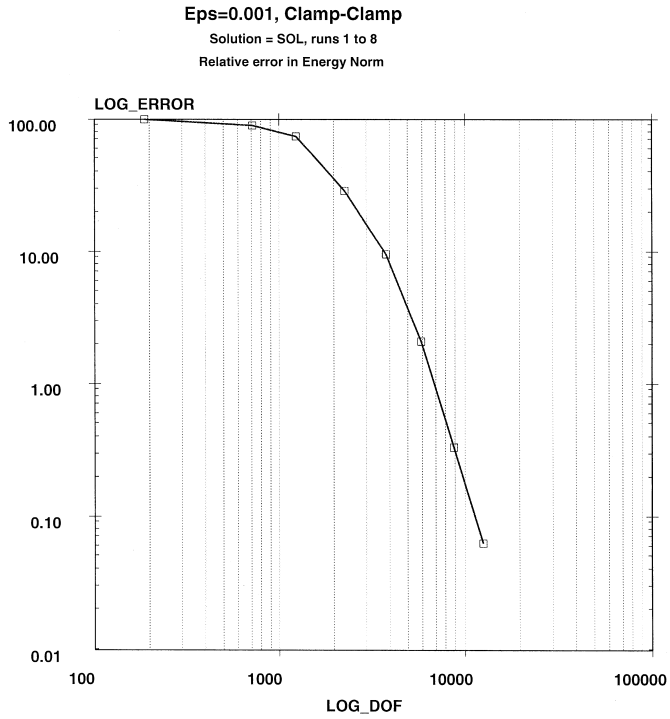

Fig. 6. Convergence rate in energy norm, ① BCs, with $2\varepsilon = 0.001$.

5.1. Visualization of boundary layers in a three-dimensional rectangular plate

A three three-dimensional p-version finite element model is constructed having two elements in the thickness direction, four elements in the x_2 direction and six elements in the x_1 direction. In the neighborhood of the edges, the mesh is graded so that there are two elements of dimension ε each. See Fig. 4 for a typical mesh for $2\varepsilon = 0.1$ and Fig. 5 for $2\varepsilon = 0.001$ and ① boundary conditions. The finite element model is constructed parametrically so that the value of 2ε may vary, and we change it from $0.1\ (= 10^{-1})$ to $0.00031622777 (= 10^{-3.5})$. Although not visible on Fig. 5, there are two elements across the thickness and two elements each of dimension ε in the neighborhood of the boundary. The p-level over each element has been increased from 1 to 8 and the trunk space has been used (Szabó and Babuška, 1991). There are 12,568 degrees of freedom at $p = 8$. An advantage of using p-version finite element methods is the possibility of having 'needle elements' in the boundary layer zone with aspect ratios as large as 10,000 without significant degradation in the numerical performance.

The convergence rate in energy norm for $2\varepsilon = 0.001$ is provided in Fig. 6 as a typical example. An *exponential convergence rate* is obtained without thickness-locking phenomenon visible (due to the use of high-order elements). The convergence of the computed data has been examined as well for increasing p-levels in order to evaluate the reliability of the numerical results.

5.1.1. Boundary layers in vertical displacement

The value of $J_2[\boldsymbol{u}], J_4[\boldsymbol{u}]$ and $J_6[\boldsymbol{u}]$, as defined in (3.12) is computed at a set of equidistant points $(s, N) = (x_1, x_2/2\varepsilon)$ along the line $x_1 = 1, 0 \leqslant x_2/2\varepsilon \leqslant 2$ for clamped boundary conditions ① and shown

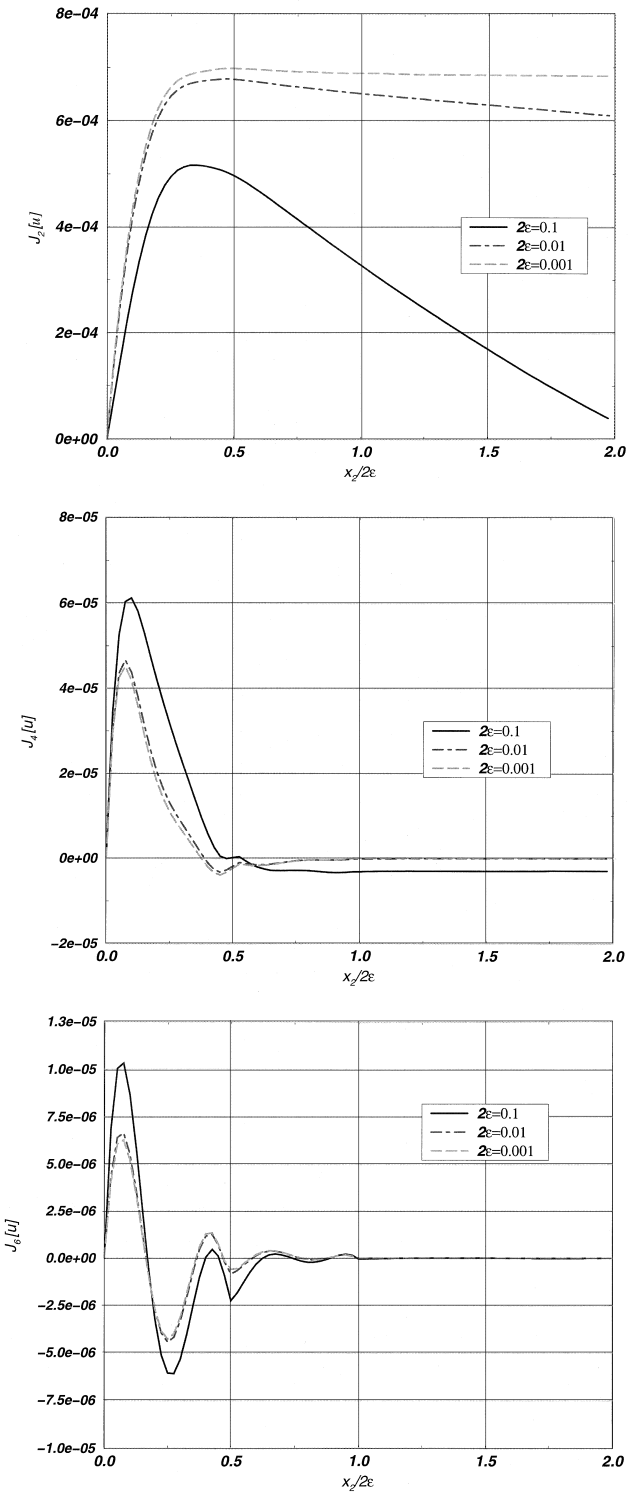

Fig. 7. $J_2[\boldsymbol{u})$, $J_4[\boldsymbol{u})$ and $J_6[\boldsymbol{u})$ for straight boundary with ①.

in Fig. 7. The graphs clearly present the existence of the boundary layer profile in the vertical displacement component in a three-dimensional domain in the vicinity of the boundary where $x_2/2\varepsilon < 1$. As expected, $J_4[\boldsymbol{u}] \to 0$ and $J_6[\boldsymbol{u}] \to 0$ as we move away from the boundary, for $\varepsilon \to 0$. The value of $J_2(\boldsymbol{u})$ tends to be a constant as we move away from the boundary because of the quadratic term X_3^2 in $\boldsymbol{v}_{\mathrm{b},3}^1$ as explained in Section 3.2.

5.1.2. Strains in the boundary layer zone

The effect of the boundary layer is visible directly on the strain components $e_{\mathrm{b},s3} = e_{13}$ or $e_{\mathrm{b},n3} = e_{23}$ as $\varepsilon \to 0$, according to (3.15) for conditions ①–③, (3.17) for condition 4 and (3.18) for conditions ⑤–⑧.

In Fig. 8 we plot $\log\,(I_{13}^{\mathrm{bl}}) = \log\,(I_{s3}^{\mathrm{bl}})$ (defined in (4.1)) vis $\log\,(2\varepsilon)$ for all boundary conditions ①–⑧ (log herein denotes $\log_{10}$). One may clearly see the boundary layer effects for boundary conditions ④, ⑤, ⑦ and ⑧ which are manifested by the nearly constant value of $\log\,(I_{s3}^{\mathrm{bl}})$ as $\varepsilon \to 0$, as predicted by the mathematical analysis. As predicted for straight boundaries, no boundary layer is visible for ③ and ⑥.

We plot in Fig. 9 the values of $\log\,(I_{23}^{\mathrm{bl}}) = \log\,(I_{n3}^{\mathrm{bl}})$ as $\varepsilon \to 0$ for all boundary conditions ①–⑧. The value of $\log\,(I_{n3}^{\mathrm{bl}})$ for ⑥ is virtually zero so that it is not shown in Fig. 9. Again, the boundary layer

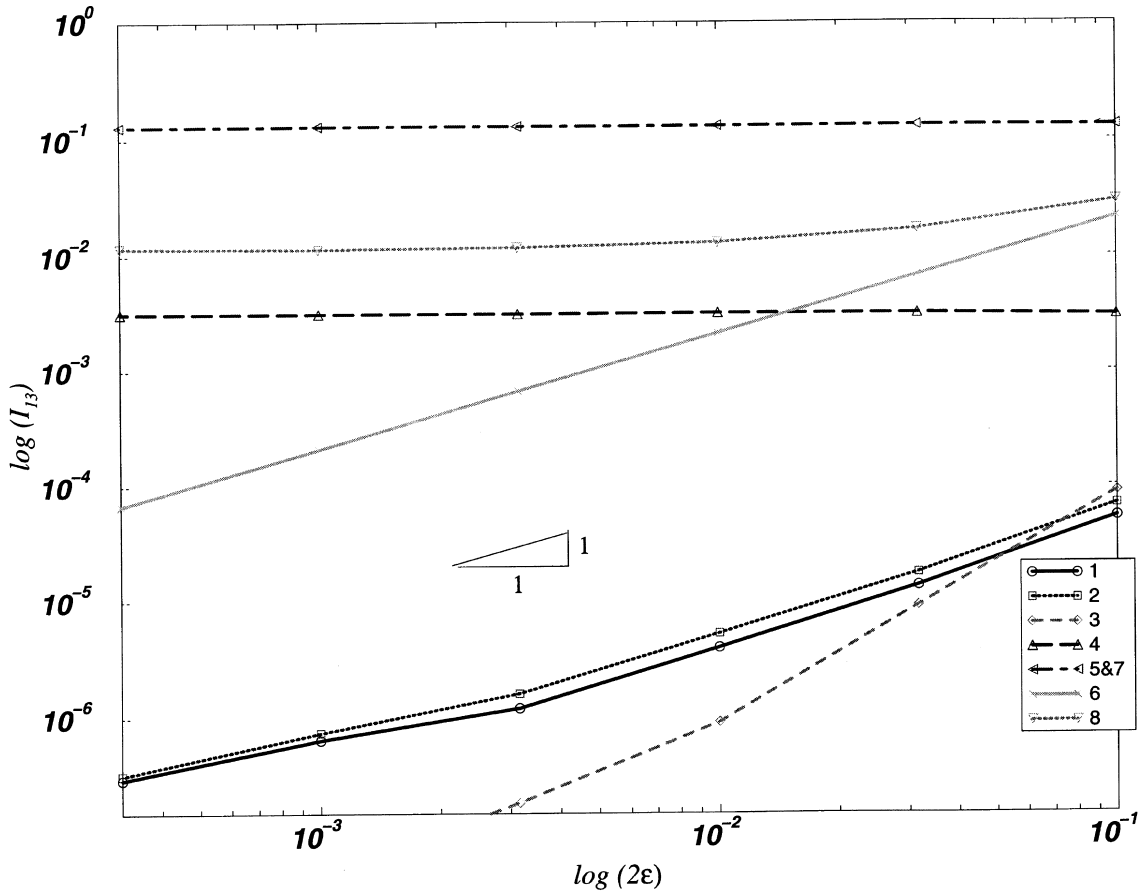

Fig. 8. $\log\,(I_{13}^{\mathrm{bl}}) = \log(I_{s3}^{\mathrm{bl}})$ vis $\log\,(2\varepsilon)$ for ①–⑧ BCs (straight boundary).

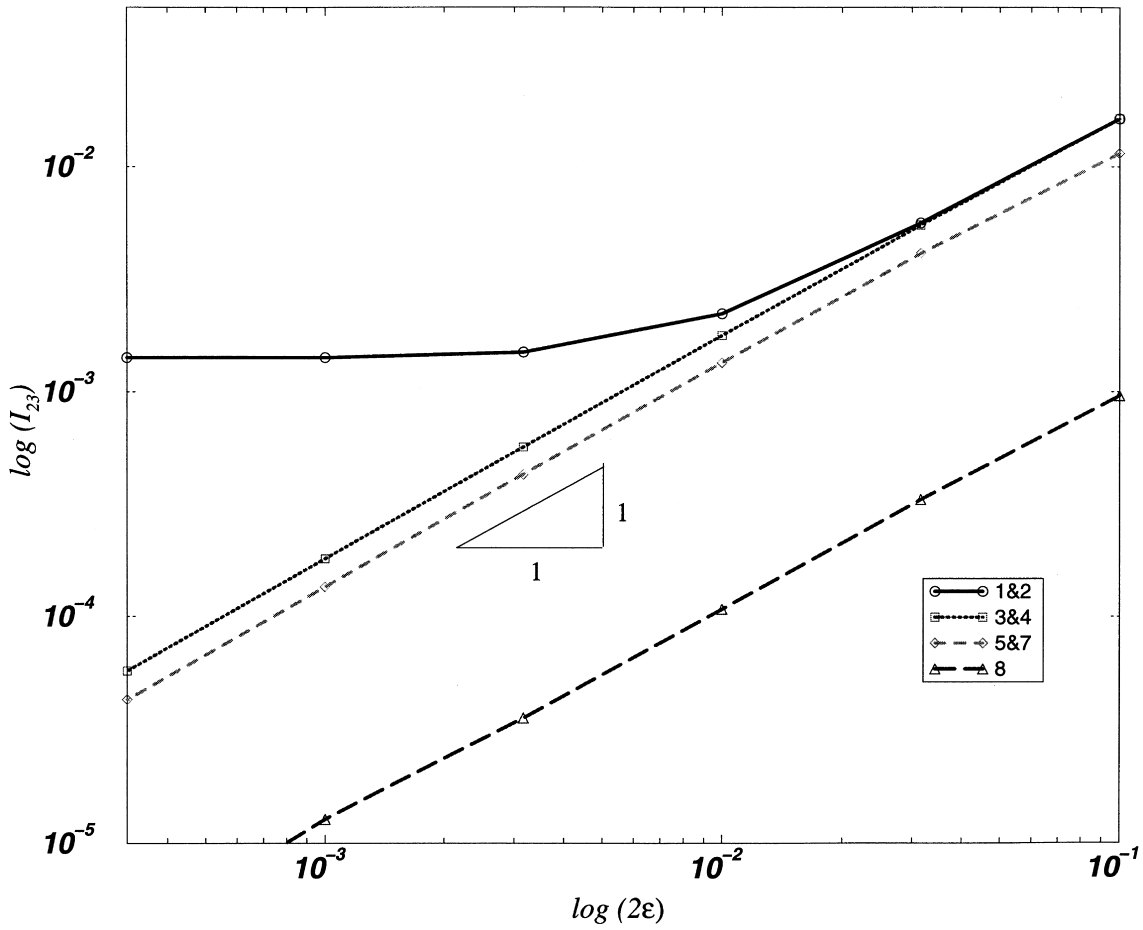

Fig. 9. log $(I_{23}^{\mathrm{bl}}) = \log(I_{n3}^{\mathrm{bl}})$ vis log (2ε) for ①–⑧ BCs (straight boundary).

effect is clearly visible for ① and ②; I_{n3}^{bl} approaches a constant value as $\varepsilon \to 0$. This is due to the $\mathcal{O}(1)$ component of the boundary layer profile, which may be smaller compared to $(\varepsilon/2)\partial_2 v_3^1$ for large values of ε, but much larger as $\varepsilon \to 0$.

5.1.3. Strains outside the boundary layer zone

For comparison purposes, we present the N-RMS norm computed outside of the boundary layer, defined in (4.2). This shows that, for all boundary conditions, both I_{13}^{out} and I_{23}^{out} are of order ε as the thickness tends to zero, due to the leading term of order ε in the strain components according to (3.10).

In Fig. 10 we plot log (I_{13}^{out}) vis log (2ε).

In Fig. 11 we plot log (I_{23}^{out}) vis log (2ε). Because (I_{23}^{out}) is nearly zero for ⑥ boundary condition, it has not been shown in Fig. 11.

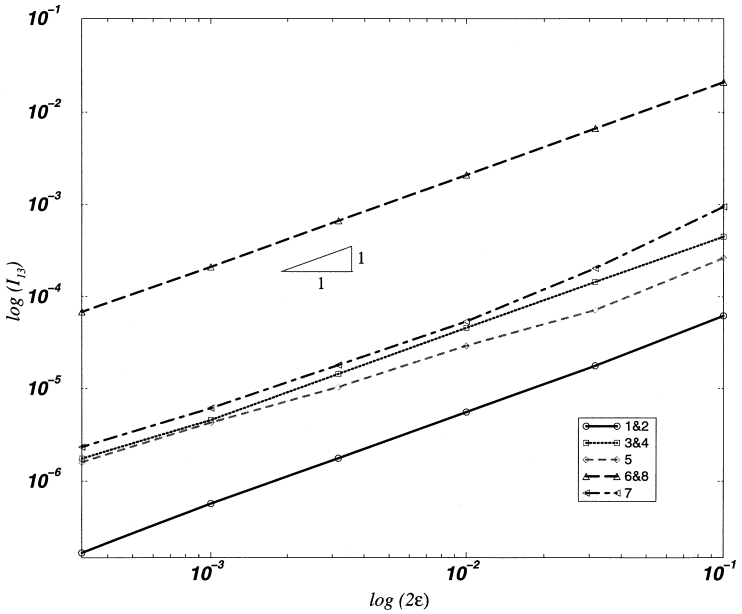

Fig. 10. log (I_{13}^{out}) vis log (2ε) for ①–⑧ BCs (straight boundary).

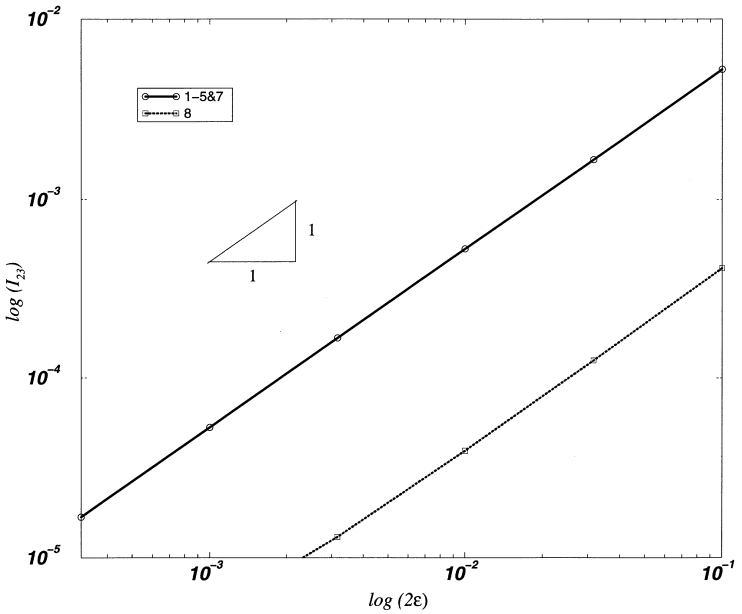

Fig. 11. log (I_{23}^{out}) vis log (2ε) for ①–⑤, ⑦ and ⑧ BCs (straight boundary).

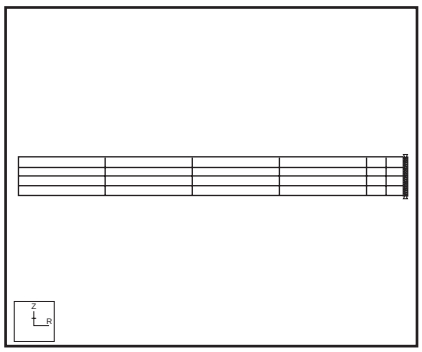

Fig. 12. Finite element mesh and boundary conditions for the circular plate $2\varepsilon = 0.1$.

5.2. Boundary layers in three-dimensional soft simply supported ④ circular plate

Consider the plate shown in Fig. 3, with soft simply supported boundary conditions $u_3 = 0$, $T_s = T_n = 0$, prescribed along the circular boundary.

Since the geometry, loading and boundary conditions are independent of θ, then we may analyze the plate as an axisymmetric model, having a two-dimensional sector of radius 1 and thickness of 2ε. The finite element mesh used in our analysis is shown in Fig. 12.

We consider the N-RMS norm of the strain component e_{n3} defined by (4.3) inside the boundary layer. In Fig. 13 we plot log (I_{n3}^{bl}) vis log (2ε). As expected, I_{n3}^{bl} is independent of ε, as $\varepsilon \to 0$ for curved

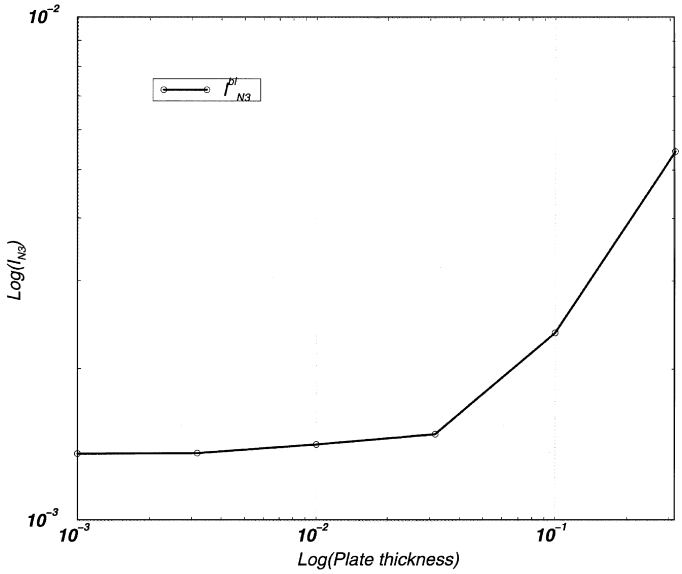

Fig. 13. log(I_{n3}^{bl}) vis log (2ε) for circular plate with ④.

boundaries, demonstrating a boundary layer profile as opposed to the case of a straight boundary. One may observe in (3.17) that e_{n3} for curved boundary is or order 1.

6. Two-dimensional formulation of hierarchic plate-models

Hierarchic plate-models have been formulated in the past ten years, and the reader is referred to Szabó and Babuška (1991), Babuška and Li (1991), Szabó and Sahrmann (1988) and Schwab (1989) for early references and Alessandrini et al. (1996, 1997) for mixed hierarchical models using the Hellinger–Reissner principle.

Here follows a short overview on hierarchic plate models in the framework of the code that we use (Stress Check User's Manual, 1996). A hierarchical family of plate models, denoted by the index d (for which its solution is defined as $\boldsymbol{u}_d^\varepsilon$) is one which satisfies:

(a) $\|\boldsymbol{u}^\varepsilon - \boldsymbol{u}_d^\varepsilon\|/\|\boldsymbol{u}^\varepsilon\| \to 0$, as $\varepsilon \to 0$. Usually the energy norm is used.
(b) If the solution $\boldsymbol{u}^\varepsilon$ is sufficiently smooth with respect to ε then:

$$\|\boldsymbol{u}^\varepsilon - \boldsymbol{u}_d^\varepsilon\|/\|\boldsymbol{u}^\varepsilon\| \leqslant C(d)\varepsilon^{\alpha(d)}$$

with $\alpha(d) > \alpha(d-1)$.
(c) For any fixed ε

$$\|\boldsymbol{u}^\varepsilon - \boldsymbol{u}_d^\varepsilon\|/\|\boldsymbol{u}^\varepsilon\| \to 0, \quad \text{as } d \to \infty$$

The displacements $\boldsymbol{u}_d^\varepsilon$ of the plate-model d are:

$$\boldsymbol{u}_d^\varepsilon = \begin{Bmatrix} \sum_{j=1}^{n_1} u_{1|j}(x_1, x_2) w_{1|j}(x_3) \\ \sum_{j=1}^{n_2} u_{2|j}(x_1, x_2) w_{2|j}(x_3) \\ \sum_{j=1}^{n_3} u_{3|j}(x_1, x_2) w_{3|j}(x_3) \end{Bmatrix}. \tag{6.1}$$

Herein d is the number of the model, which coincides with the highest polynomial degree describing the displacement components. We will be considering the hierarchic plate-model family implemented in the finite element code Stress Check[2] (Stress Check User's Manual, 1996), for which (note that this code aims at solving the bending equations whereas membrane, or stretching, models are variants of generalized plane-stress situations which are not addressed here).

The first hierarchical plate-model $d = 1$ with the special material matrix given in Stress Check User's Manual (1996) is exactly the R–M model, where the shear correction factor is chosen so as to minimize the error in the energy norm:

$$\text{shear corr. factor} = \frac{5}{6(1-\nu)}$$

[2] Stress Check is a trade mark of Engineering Software Research and Development, Inc., Clayton Plaza, Suite 204, 7750 Clayton Rd., St Louis, MO, USA.

Table 4
Hierarchic plate-model definitions

d	(n_1, n_2, n_3)	Non-zero $w_1 = w_2$	Non–zero w_3
1	(1, 1, 1)	$w_{1\|1} = w_{2\|1} = x_3$	$w_{3\|1} = 1$
2	(1, 1, 2)	$w_{1\|1} = w_{2\|1} = x_3$	$w_{3\|1} = 1, w_{3\|2} = x_3^2$
3	(2, 2, 2)	$w_{1\|1} = w_{2\|1} = x_3$ $w_{1\|2} = w_{2\|2} = x_3^3$	$w_{3\|1} = 1, w_{3\|2} = x_3^2$
4	(2, 2, 3)	$w_{1\|1} = w_{2\|1} = x_3$ $w_{1\|2} = w_{2\|2} = x_3^3$	$w_{3\|1} = 1, w_{3\|2} = x_3^2$ $w_{3\|3} = x_3^4$
5	(3, 3, 3)	$w_{1\|1} = w_{2\|1} = x_3$ $w_{1\|2} = w_{2\|2} = x_3^3$ $w_{1\|3} = w_{2\|3} = x_3^5$	$w_{3\|1} = 1, w_{3\|2} = x_3^2$ $w_{3\|3} = x_3^4$

For $d = 2$ the shear correction factor is given in Stress Check User's Manual (1996) and for $d \geqslant 3$ no shear correction factor in the material matrix is needed.

Remark 6.1 *The K–L plate-model is not a member of the hierarchical family. It represents in a decoupled system the solution of the bending equation for* ξ_3:

$$D\Delta_*^2\zeta_3(x_1, x_2) = f_3(x_1, x_2), \quad D\frac{E(2\varepsilon)^3}{12(1-\nu)^2},$$

and a membrane equation for $\boldsymbol{u}_*$, *and this solution is unable to manifest boundary layers.*

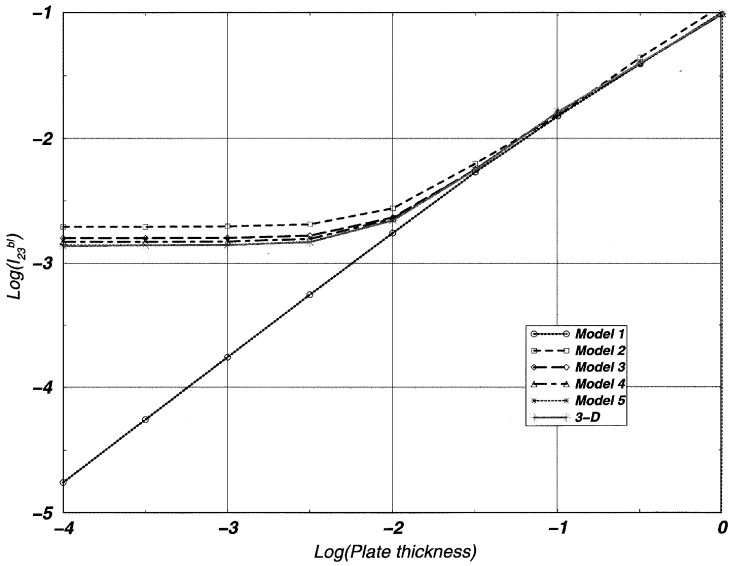

Fig. 14. Three-dimensional vis two-dimensional plate models: $\log(I_{23}^{\mathrm{bl}})$ vis $\log(2\varepsilon)$ for ①.

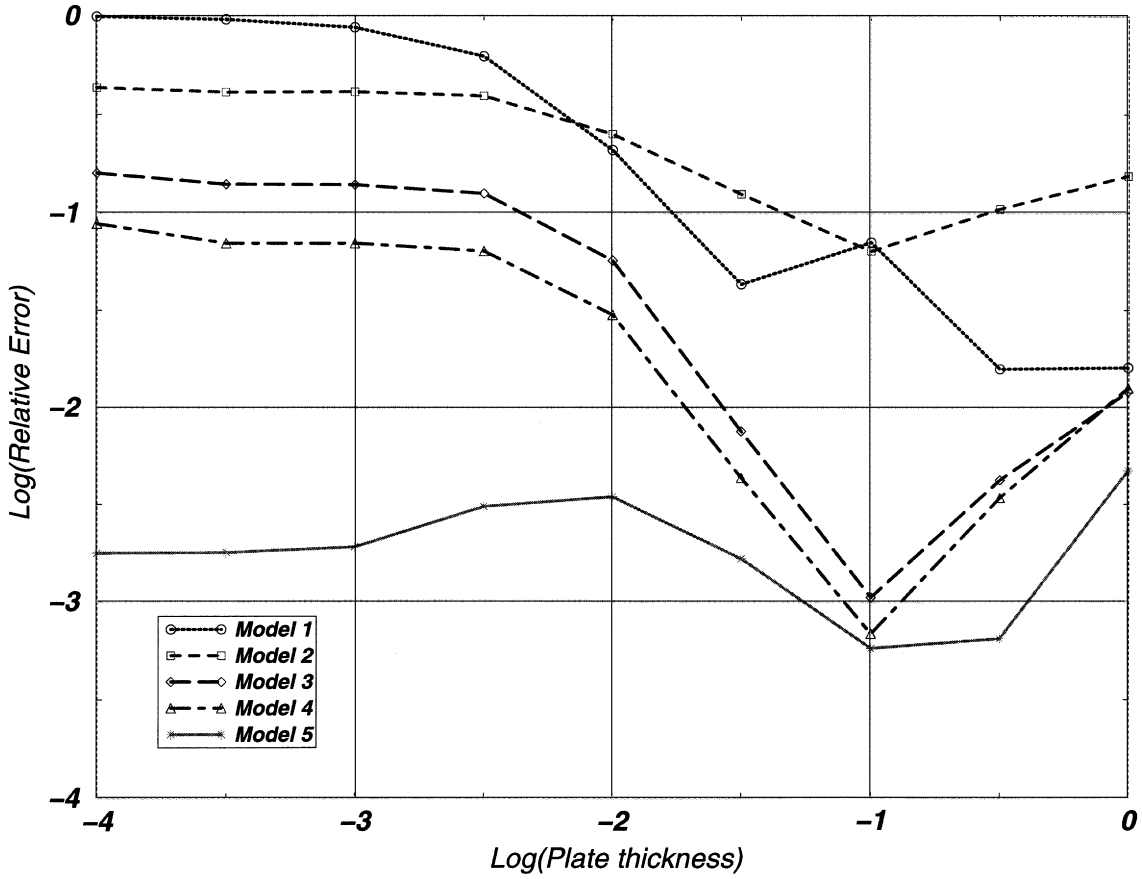

Fig. 15. log of rel. err. in I_{23}^{bl} between the three-dimensional and two-dimensional plate models as $\varepsilon \to 0$ for ①.

7. Numerical tests for comparing three-dimensional and two-dimensional plate models

Of major interest is the question whether the various hierarchic plate models are able to capture the boundary layers present in three-dimensional domains. To address this question we consider the five hierarchic plate models having $d = 1, 2, 3, 4$ and 5, and we denote them by model 1, 2, 3, 4 and 5 correspondingly. For the plate models, we consider the mid-surface of the three-dimensional domain, with a vertical pressure of a magnitude ε^2 applied on it. On the two-dimensional surface we lay a finite element mesh identical to the mesh on any plane (x_1, x_2) of the three-dimensional model presented in Fig. 4. The first plate-model $d = 1$ with a special material matrix is the R–M model. For this R–M model, the hard clamped boundary conditions are applied by imposing zero displacements in all directions, which implies zero slope normal and tangential to the plate boundary. In all plate models the convergence rate in energy norm is exponential as well as the convergence rate of the strains.

Herein we analyze only three kinds of boundary conditions along a straight edge: ①, ⑥ and ⑧, and compare the plate model's boundary layer against the three-dimensional domain boundary layer.

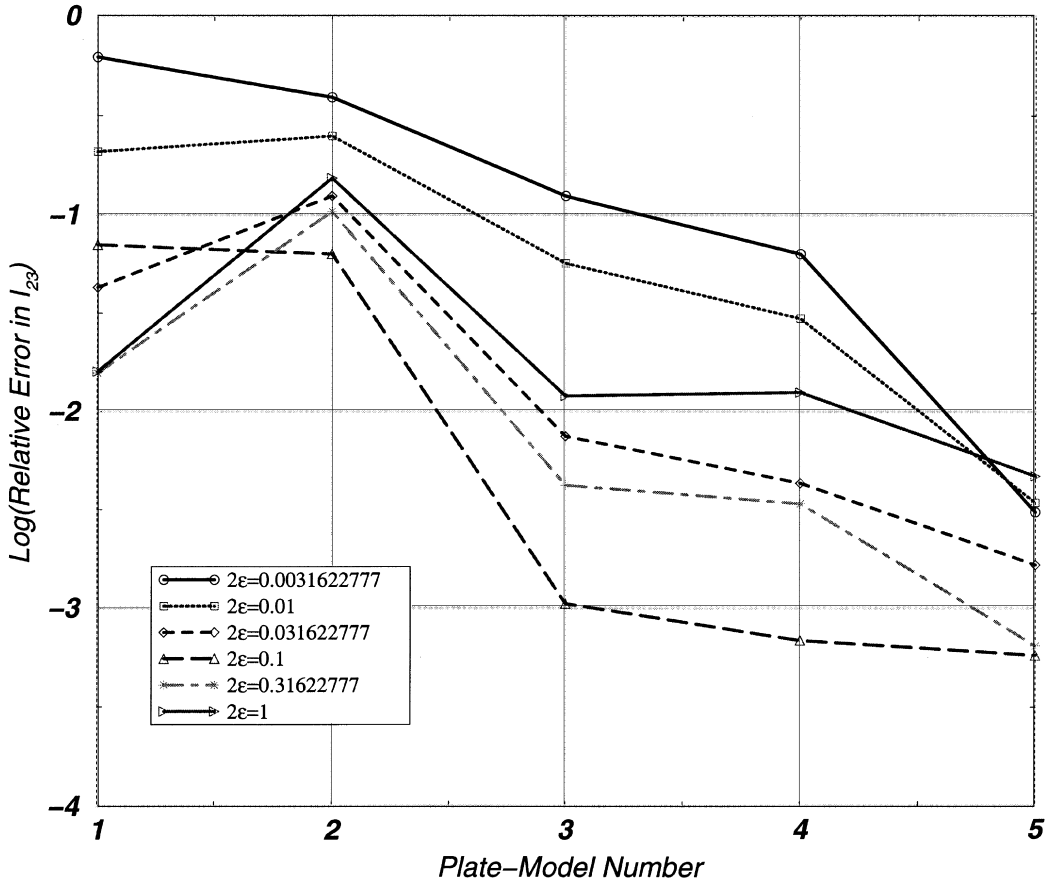

Fig. 16. log of rel. err. in I_{23}^{bl} between the three-dimensional and two-dimensional plate models as the model number is increased for ①.

7.1. Hard clamped plate ①

The value of log (I_{23}^{bl}) for the various two-dimensional plate models is plotted against the value obtained for the three-dimensional domain as $\varepsilon \to 0$ in Fig. 14. One may notice that the R–M plate model (model 1) cannot mimic the boundary layer term. However, as we increase the order of hierarchic plate models, a better approximation of the boundary layer is obtained. A more pronounced difference between the three-dimensional solution and the two-dimensional plate models is visible once we plot in Fig. 15 the relative error in I_{23}^{bl} between the three-dimensional domain and the plate models:

$$\text{Relative Error} \stackrel{\text{def}}{=} \left| \frac{I_{23}^{\mathrm{bl}}|_{3\text{–D}} - I_{23}^{\mathrm{bl}}|_{2\text{–D model}}}{I_{23}^{\mathrm{bl}}|_{3\text{–D}}} \right|$$

as $\varepsilon \to 0$. Fig. 15 shows how well the boundary layer term in the fully three-dimensional solution is represented by the various plate models as $\varepsilon \to 0$. It is also interesting to inspect the relative error in I_{23}^{bl}

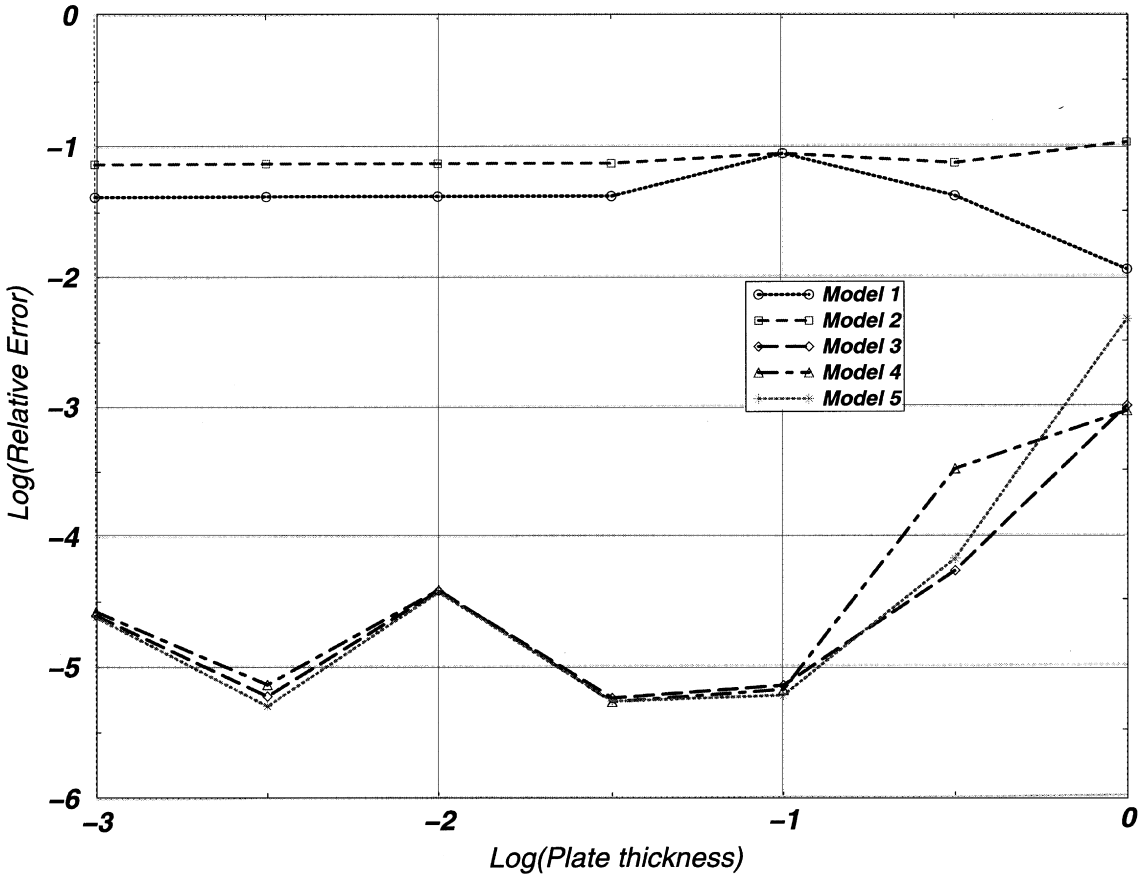

Fig. 17. log of relative error in I_{23}^{out} between the three-dimensional and two-dimensional plate models as $\varepsilon \to 0$ for ①.

between the three-dimensional and two-dimensional plate models as the model number is increased, for the different thicknesses. This is shown in Fig. 16. One may notice that plate model 2 does not always approximate better the boundary layer zone as compared to the R–M plate model. As the plate hierarchy increases, the better the approximability of boundary layers, independent of the thickness.

If one is interested in the outer field (away from the boundary layer zone), the relative error in I_{23}^{out} can be analyzed. In Fig. 17 we plot the relave error in I_{23}^{out} between the three-dimensional model and the various plate models as $\varepsilon \to 0$. Away from the boundary layer a much smaller relative error is visible.

7.2. Comparing three-dimensional and two-dimensional plate models—free plate ⑧

Herein we examine the value of log (I_{23}^{bl}) associated with the boundary layer of the free boundary. It is plotted in Fig. 18 for various two-dimensional plate models against the value obtained for the three-dimensional domain as $\varepsilon \to 0$. In this case, even the first plate model (R–M), is very close to the three-

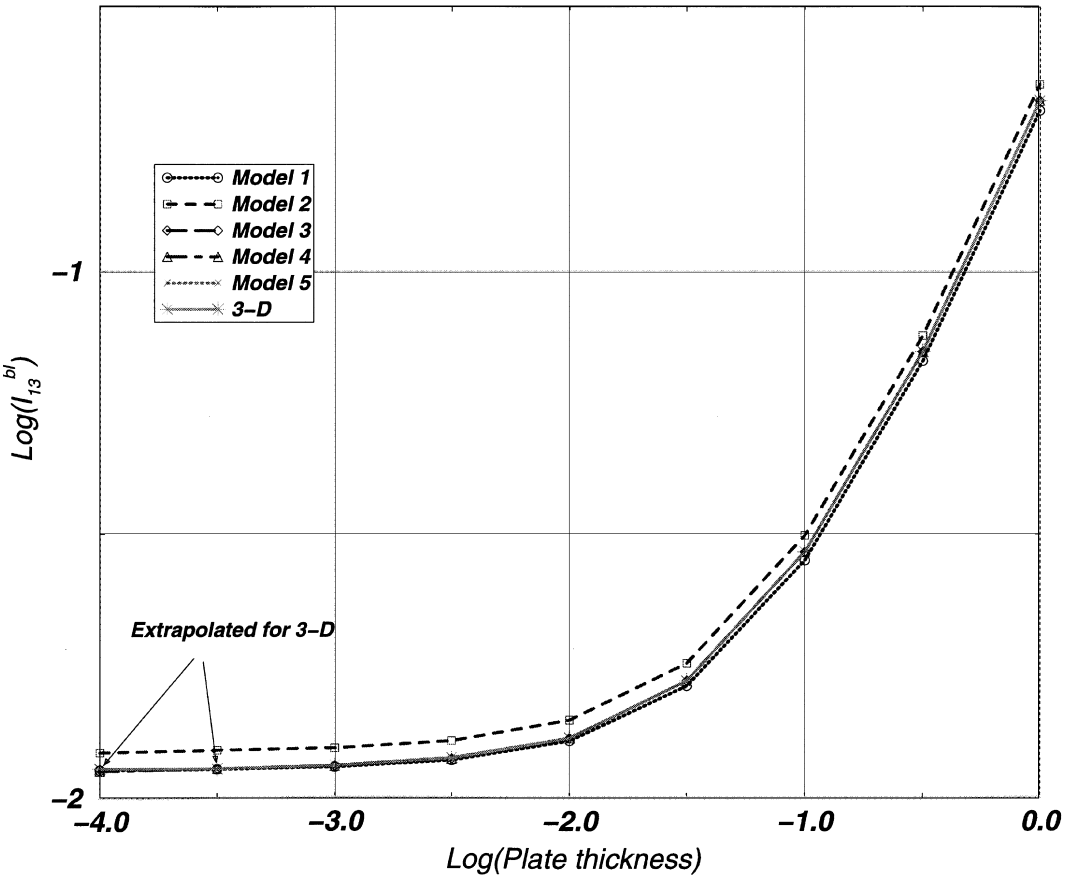

Fig. 18. Three-dimensional vis two-dimensional plate models: log (I_{13}^{bl}) vis log (2ε) for ⑧.

dimensional solution, capturing the boundary layer term well. Due to numerical errors in the three-dimensional models at $2\varepsilon < 10^{-3.5}$ we were not able to compute I_{13}^{bl} and I_{13}^{out} reliably, so that this value is extrapolated using the previous two results in Figs. 18 and 20 for the smallest two values of ε. In Fig. 19 we inspect the relative error in I_{13}^{bl} between the three-dimensional and two-dimensional plate models as the model number is increased, for the different thicknesses. Again, one may notice that plate model 2 does not always approximate better the boundary layer zone as compared to the R–M plate model.

The value of I_{13}^{out} (away from the boundary layer zone) for the three-dimensional model and the various plate models as $\varepsilon \to 0$ is plotted in Fig. 18. Again, one notices the very good agreement between the various plate models and the fully three-dimensional solution away from the boundary layer.

7.3. Comparing three-dimensional and two-dimensional plate models—slide plate ⑥

Herein we examine the value of log (I_{13}^{bl}) associated with the boundary layer of the sliding boundary condition. As predicted this value should approach zero as $\varepsilon \to 0$, since no boundary layer profile exists,

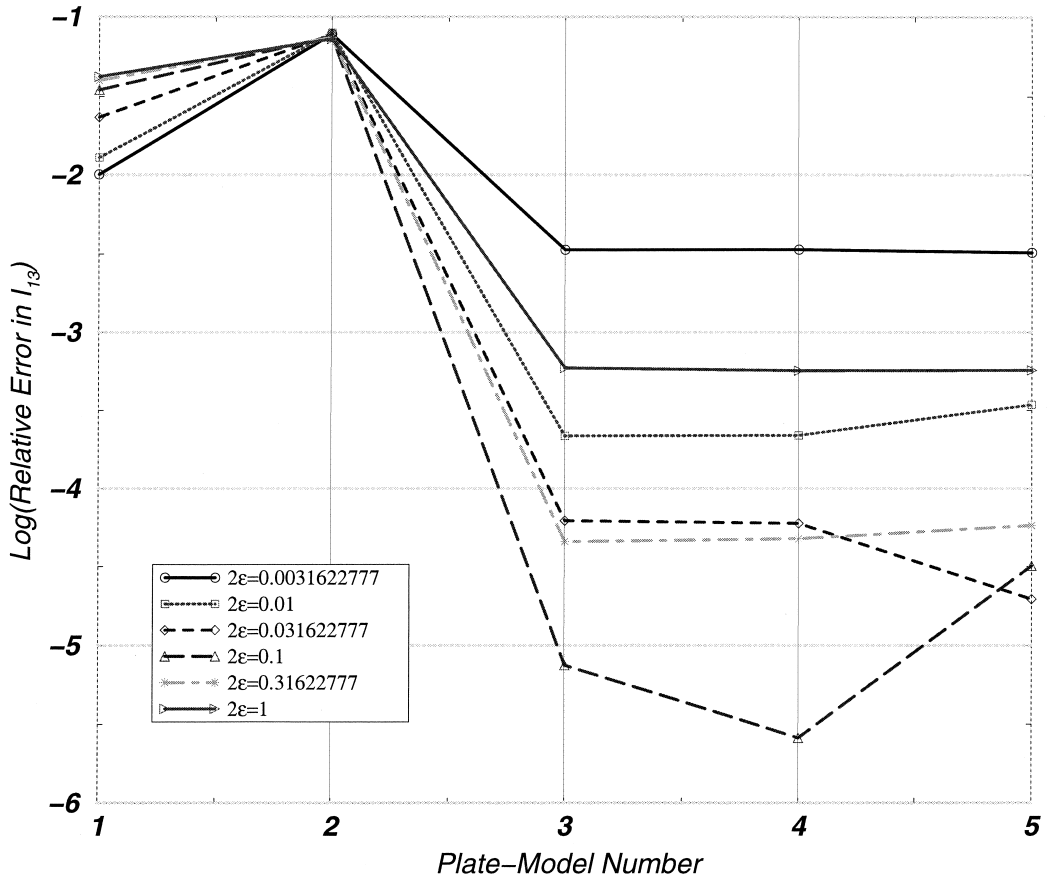

Fig. 19. log of rel. err. in I_{13}^{bl} between the three-dimensional and two-dimensional plate models as the model number is increased for ⑧.

therefore the same behavior is expected from the various two-dimensional plate models. Fig. 21 shows $\log I_{13}^{bl}$ for various two-dimensional plate models against the value obtained for the three-dimensional domain as $\varepsilon \to 0$. In this case, all plate models mimic the three-dimensional solution due to non-existence of boundary layers.

8. Summary and conclusions

The solution of the elasticity problem in three-dimensional thin domains (having a thickness of 2ε) has been explicitly provided as an asymptotic series in ε. It has terms which exist in the boundary layer zone, which is of magnitude ε, and vanish away from it. This enables us to identify, and more importantly quantify, the quantities which are rapidly changing in the boundary layer zone. Numerical

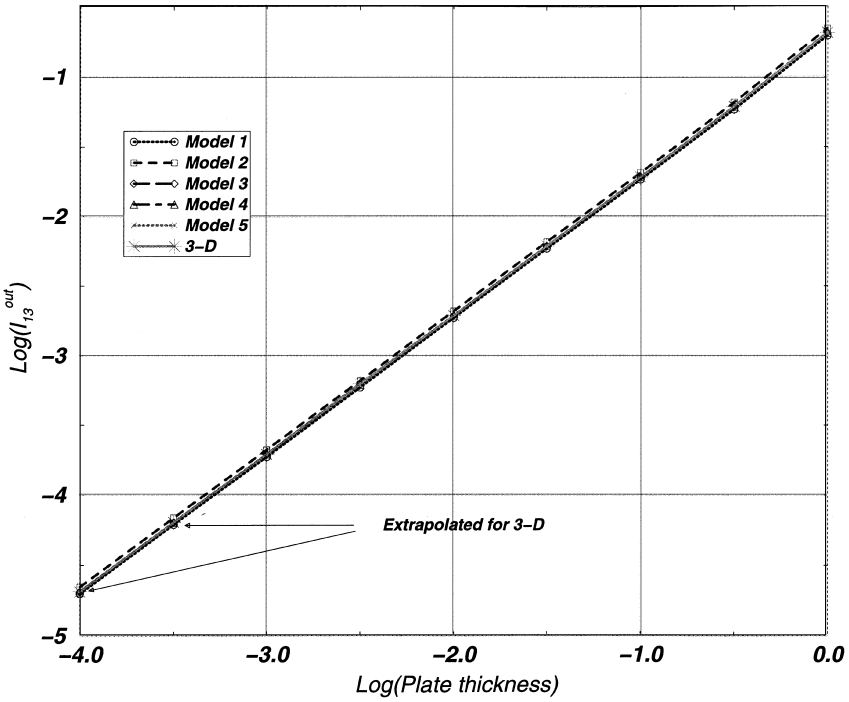

Fig. 20. Three-dimensional vis two-dimensional plate models: log (I_{13}^{out}) vis log (2ε) for ⑧.

experiments using the *p*-version of the finite element method, show that some of the strain components (thus the associated stress components) may be solely influenced by the boundary layer terms in the vicinity of boundary layers.

We also examine how well the various hierarchic plate models approximate the three-dimensional solution as $\varepsilon \to 0$. It has been demonstrated that for some boundary conditions, ⑧ for example, even the lowest member of the hierarchic plates family (R–M model) is able to capture the right boundary layer behavior, whereas for other boundary conditions, ① for example, the R–M plate model misses its behavior for some of the strain components. When no boundary layers exist in the three-dimensional solution, ⑥ for example, then plate models mimic the three-dimensional solution in the 'boundary layer' zone well. In all examined cases as we increase the hierarchic order of the plate models we converge to the right boundary layer representation.

The three-dimensional solution in the outer zone (away from the boundary layer) is much better approximated by the various plate models. It is important to note that all finite element models used have a proper mesh refinement towards the boundary layer zone. An improper mesh layout may cause numerical pollution errors from the boundary layer zone into the whole plate, thus even if the boundary layer solution is not of interest, a proper mesh layout is necessary to ensure control of numerical errors (Suri et al., 1998).

There might be pathological cases in which the boundary layer terms will highly influence the solution away from the boundary, a subject which is under investigation.

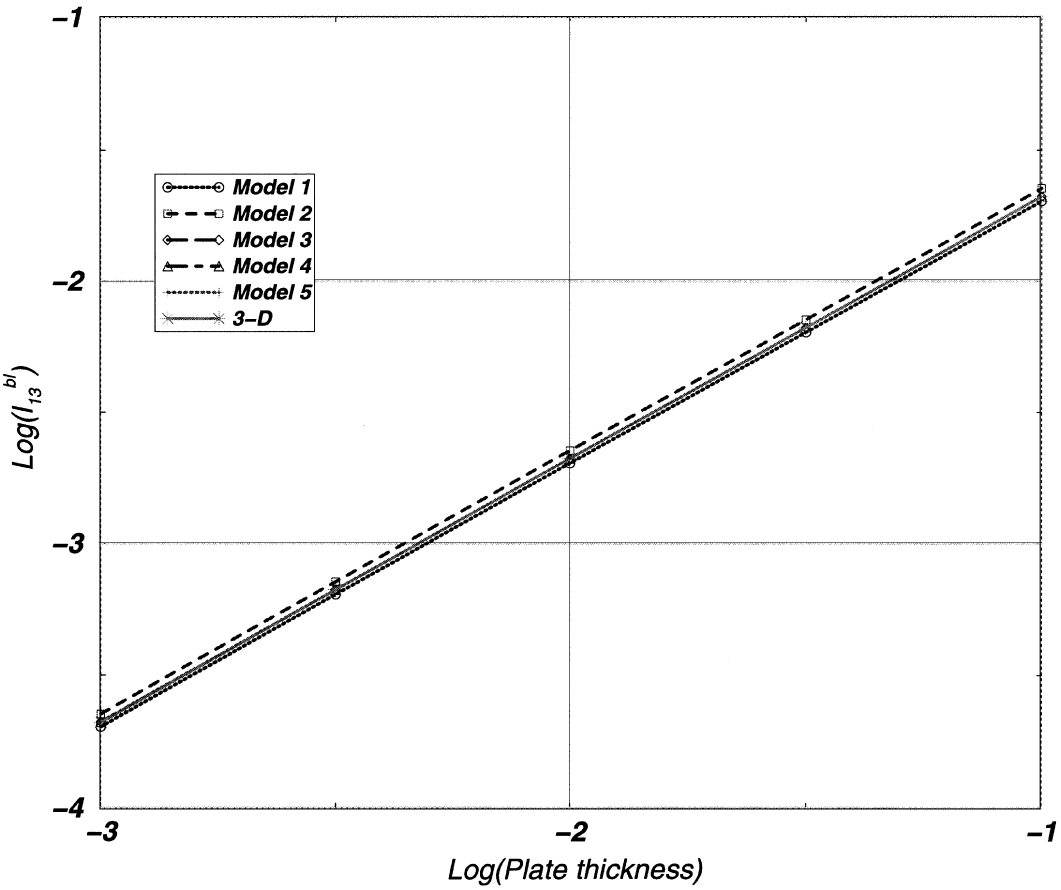

Fig. 21. Three-dimensional vis two-dimensional plate models: log (I_{13}^{bl}) vis log (2ε) for ⑥.

References

Stress Check User's Manual, Release 2.0, 1996. ESRD, St Louis, USA.

Alessandrini, S.M., Arnold, D.N., Falk, R.S., Madureira, A.L., 1996. Derivation and justification of plate models by variational methods. In: Proceeding of the summer seminar of the Canadian Mathematical Society on 'Plates and shells: from mathematical theory to engineering practice', CRM Proceeding and Lecture Notes, Quebec.

Alessandrini S.M., Arnold, D.N., Falk, R.S., Madureira, A.L., 1997. Dimensional reduction based on mixed variational principles. In: Bernadou, M, Ciarlet, P.G., Viaño, J.M. (Eds.), Shells: mathematical modelling and scientific computing. Cursos e congresos da Universidade de Santiago de Compostela, pp. 25–28.

Arnold, D., Falk, R., 1990a. Edge effects in the Reissner–Mindlin plate model. In: Noor, A., Belytschko, T., Simo, J. (Eds.), Analytical and Computational Models for Shells. American Society of Mechanical Engineers, New York, pp. 71–90.

Arnold, D.N., Falk, R.S., 1990b. The boundary layer for the Reissner–Mindlin plate model. SIAM J. Math. Anal. 21 (2), 281–312.

Arnold, D.N., Falk, R.S., 1996. Asymptotic analysis of the boundary layer for the Reissner–Mindlin plate model. SIAM J. Math. Anal. 27 (2), 486–514.

Babuška, I., Li, L., 1992a. The problem of plate modelling: Theoretical and computational results. Comput. Meth. Appl. Mech. Engrg 100, 249–273.

Babuška, I., Li, L., 1991. Hierarchic modeling of plates. Comput. & Structures 40, 419–430.

Babuška, I., Li, L., 1992b. The *h-p*-version of the finite element method in the plate modelling problem. Comm. Appl. Numer. Meth. 8, 17–26.

Ciarlet, P.G., 1990. Plates and Junctions in Elastic Multi-Structures: An Asymptotic Analysis. R.M.A., Vol. 14. Masson and Springer-Verlag, Paris and Heidelberg.

Dauge, M., Gruais, I., Rössle, A., 1997. The influence of lateral boundary conditions on the asymptotics in thin elastic plates I & II. Prépublications 97-28 & 97-29, IRMAR 1997. On the web: http://www.maths.univ-rennes1.fr/ ~ dauge/.

Dauge, M., Gruais, I., Rössle, A., 1998. The influence of lateral boundary conditions on the asymptotics in thin elastic plates. To appear in SIAM Journal of Math. Anal.

Friedrichs, K.O., Dressler, R.F., 1961. A boundary-layer theory for elastic plates. Comm. Pure Appl. Math. 14, 1–33.

Schwab, C., 1989. The dimension reduction method. Ph.D. thesis, University of Maryland, College Park.

Schwab, C., Suri, M., 1996. The *p* and *hp* versions of the finite element method for problems with boundary layers. Math. Comp. 65, 1403–1429.

Suri, M., Schwab, C., Xenophontos, C., 1998. The *hp* finite element method for problems in mechanics with boundary layers. Comp. Meth. Appl. Mech. Engrg 157, 311–333.

Szabó, B., Babuška, I., 1991. Finite Element Analysis. Wiley, New York.

Szabó, B., Sahrmann, G., 1998. Hierarchic plate and shell models based on *p*-extension. Int. J. Numer. Meth. Engrg 26, 1855–1881.